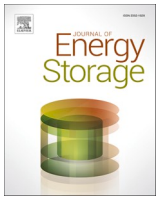
Journal of Energy Storage 179 (2026) 123852



Contents lists available at ScienceDirect

Journal of Energy Storage

journal homepage: www.elsevier.com/locate/est



Review article

Carnot battery: Improving the round-trip efficiency and reducing the levelized cost of storage

Anbu Chen [a,b], Huan Liu [c], Qiuru Dong [a,b], Jinliang Xu [a,b], Jian Xie [a,b,*]

[a] Beijing Key Laboratory of Multiphase Flow and Heat Transfer for Low Grade Energy Utilization, North China Electric Power University, Beijing, 102206, China
[b] Key Laboratory of Power Station Energy Transfer Conversion and System of Ministry of Education, North China Electric Power University, Beijing, 102206, China
[c] National Institute of Energy Development Strategy, North China Electric Power University, Beijing, 102206, China

ARTICLE INFO

Keywords:
Carnot battery
Thermal energy storage
Long-duration energy storage
Heat pump
Techno-economic assessment

ABSTRACT

As an innovative long-duration energy storage technology, Carnot battery was developed rapidly in recent years. Here, the investigations and commercial applications of Carnot battery are comprehensively reviewed. The influence on techno-economic indexes is mainly discussed. The round-trip efficiency (RTE) of Carnot battery is selected as the technical evaluation index, which reflects the overall efficiency of the three core processes, including charging, energy storage and discharging. Meanwhile, the levelized cost of storage (LCOS) is chosen as the economic evaluation index because it comprehensively considers the investment, operation and maintenance cost over its total lifetime. From the perspectives of system, thermal-integrated pumped thermal energy storage (TI-PTES) is identified as the potential configuration with high RTE and low LCOS. From the view of key components, increasing isentropic efficiencies of turbomachinery and decreasing the pinch point temperature difference of heat exchanger are the effective pathways to rise RTE and reduce LCOS. In future, dynamic operation of Carnot battery and advanced control strategies need to be especially concerned, ensuring high RTE in all operating states and low LCOS with benefits from flexible operation.

Nomenclature

A	Area [m^2]
C	Cost [$]
E	Electric energy [Wh]
Q	Quantity of heat [J]
T	Temperature [K]
V	Volume [m^3]
W	Electrical work [J]
i	Run time [year]
r	Discount rate [%]
f	Correction factor [−]

Abbreviations

B-PTES	Brayton cycle-based Pumped Thermal Energy Storage
COP	Coefficient of Performance
HP	Heat Pump
LAES	Liquid Air Energy Storage
LCOS	Levelized Cost of Storage
NMPC	Nonlinear Model Predictive Control
ORC	Organic Rankine Cycle
PCMs	Phase Change Materials
PTES	Pumped Thermal Energy Storage
R-PTES	Rankine cycle-based Pumped Thermal Energy Storage
RTE	Round-Trip Efficiency
SC-PTES	Stirling cycle-based Pumped Thermal Energy Storage
TES	Thermal Energy Storage

Greek

η	Efficiency [−]
ρ	Density [kg/m^3]

Subscript

ann	Annual
c	Carnot

* Corresponding author at: Beijing Key Laboratory of Multiphase Flow and Heat Transfer for Low Grade Energy Utilization, North China Electric Power University, Beijing, 102206, China.
E-mail address: xiejian90@ncepu.edu.cn (J. Xie).

https://doi.org/10.1016/j.est.2026.123852
Received 25 February 2026; Received in revised form 7 June 2026; Accepted 21 July 2026
Available online 30 July 2026
2352-152X/© 2026 Elsevier Ltd. All rights are reserved, including those for text and data mining, AI training, and similar technologies.

e	Energy
ele	Electricity
gen	Generation
HE	Heat engine
hx	Heat exchanger
idea	Ideal
in	Input
inv	Investment
out	Output
OM	Operation and maintenance
p	Pressure
rt	Round-trip
st	Storage

1. Introduction

To reduce the emissions of carbon dioxide and limit the global warming, renewable energy is encouraged to replace the fossil energy by almost all countries. Under such background, the technologies of solar panel and wind turbine are developed rapidly, which induces falling price and surging installed electricity capacity. In 2025, the global installed electricity capacity of solar energy reached to 2750 GW, which exceeded that of coal-fired power plant for the first time since the industrial revolution. Thus, the Journal of Science name the renewable energy surge as the 2025 Breakthrough of the Year [1]. However, the intermittency and volatility of surged renewable energy bring challenge to the stable and safe operation of power systems [2]. To cope with such challenge, developing large-scale and long-duration energy storage technologies has become increasingly urgent [3].

Electrical energy is difficult to be stored directly. Thus, energy storage also means energy conversion between the electrical energy and other energy. The energy conversion between electrical and chemical energy is the simple and efficient to storge energy by traditional batteries [4]. However, traditional batteries face problems for large-scale and long-duration energy storage, including limited capacity due to the using of precious metals [5–7], fire risk during operation due to the using of flammable electrolyte [8–10], and pollution risk after retire due to the using of heavy metals and toxic organic compound [11,12].

To address the above problems, the earliest Carnot battery concept was proposed by Marguerre in 1924 [13] and has attracted growing attention in recent years (see Fig. 1(a)). Carnot battery is a physical energy storage technology based on thermodynamic cycles, involving energy conversion between electrical and thermal energy. Fig. 1(b) illustrates the fundamental operating principle of Carnot battery. When the renewable energy power generation is in surplus, electrical energy drives a heat pump cycle to upgrade and store thermal energy. It is the charge process of electricity. When electrical power is in shortage, a heat engine cycle is activated to convert the stored thermal energy back into electricity. It is the discharge process of electricity [14].

In Carnot battery, the energy is stored in form of heat with natural substances or common chemicals. It meets the demand of large-scale and long-duration energy storage and has advantage of safety during operation and after retire [15–17]. However, the grades of electric power and thermal energy behave significant difference. To maintain high efficiency of energy utilization, various configurations of thermodynamic cycles were proposed and developed for Carnot battery [18]. Various operating parameters of key components were also discussed and optimized in the past investigations [19,20]. On the other hand, the cost of Carnot battery attracted special attention in commercial applications due to huge investment for large-scale energy storage [17,21,22].

Here, the technological and economic performance of Carnot battery are reviewed from the perspectives of both system and key components. This paper is structured as follows. Section 2 introduces various configurations and application scenarios of Carnot battery. Section 3 describes key components of Carnot battery and their optimization potential for performance improvement and cost reduction. Section 4 defines the round-trip efficiency (RTE) and levelized cost of storage (LCOS) as the technical and economic evaluation index, respectively. More importantly, the influences of operating parameters on RTE and LCOS are discussed from the perspectives of configuration and key components. Section 5 reviews the commercial applications of Carnot battery and current values of RTE and LCOS. Section 6 summarizes the main conclusions and prospects.

2. Carnot battery configurations

The Carnot battery is the important system to implement energy conversion between electrical and thermal energy. Therefore, systematic investigation of its configurations enables holistic performance enhancement and cost reduction. Moreover, such research fosters the development of novel configurations, thereby broadening the operational flexibility and application scope of Carnot batteries across diverse thermal and electrical infrastructure contexts.

2.1. Overview of Carnot battery configurations

The configuration of Carnot battery is diverse (see Fig. 2 for a classification of Carnot battery configurations). This paper adopts the perspective of Dumont et al. (2020), who regard liquid air energy storage (LAES) as a form of Carnot battery [18]. The main configurations of Carnot batteries include pumped thermal energy storage based on the Brayton, Rankine, or Stirling cycle, and thermal-integrated systems that incorporate heat sources at different temperature levels. Derivative configurations such as LAES—which uses liquid air as both the working fluid and cold storage medium—and thermochemical energy storage systems, exemplified by the Lamm–Honigmann process, demonstrate significant application potential in large-scale energy storage, industrial waste heat recovery, and integrated energy systems [23].

2.2. Brayton cycle-based Carnot battery

Brayton cycle-based Carnot battery, commonly referred to as Brayton cycle-based pumped thermal energy storage (B-PTES), utilizes gases such as carbon dioxide, argon, or air as the working fluid [24–26]. These systems achieve the power-to-heat-to-power energy conversion through thermodynamic processes of gas compression and expansion, and typically require operating temperatures exceeding 500 °C [27]. As illustrated in Fig. 3, the configuration primarily comprises three variants: the basic cycle (shown in black), the regenerative configuration (in orange), and the thermal-integrated configuration that incorporates an external heat source (in red).

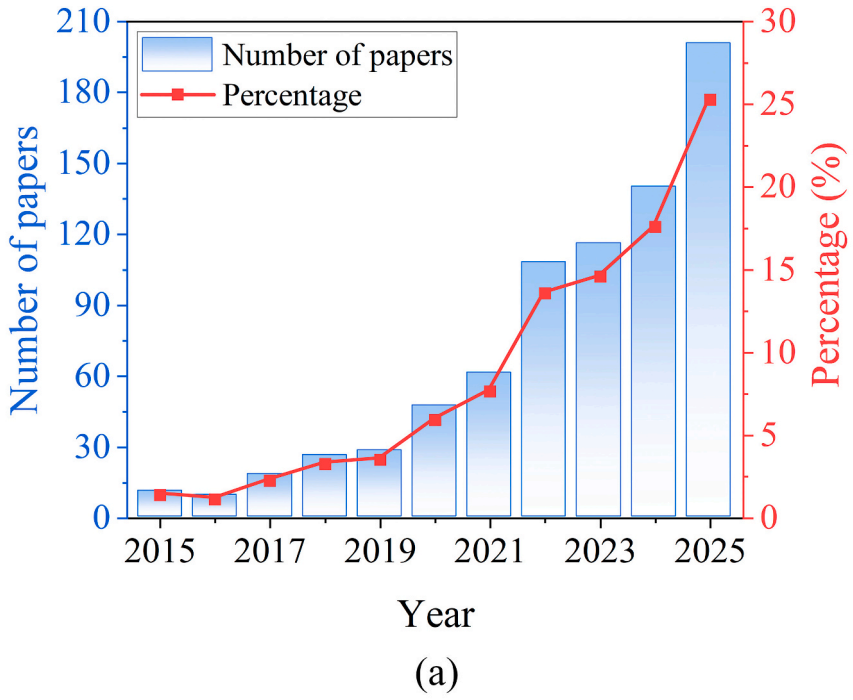
2.2.1. Basic Brayton cycle

The basic cycle configuration represents the fundamental approach to achieving power-to-heat-to-power conversion. During the charging process, heat is released through gas compression and subsequent condensation, and is typically stored in packed beds or molten salt tanks [28–30]. In the discharging phase, electricity is generated via heat absorption and gas expansion. While this configuration operates on a simple principle, it suffers from significant irreversible heat transfer losses as a result. Consequently, drawing upon mature thermal power generation technologies, regenerators have been successfully integrated into Carnot battery [24,30,31].

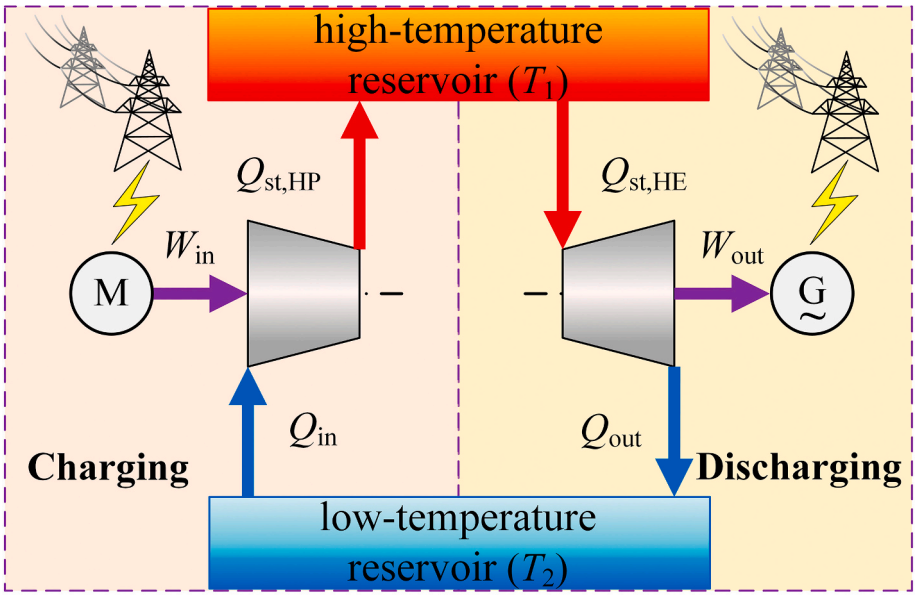
2.2.2. Regenerative Brayton cycle

This configuration enables internal heat recovery by incorporating a regenerator, which significantly reduces the temperature difference between the working fluid and the external thermal storage tank during heat exchange, thereby minimizing exergy losses [24,32]. Research indicates that adding a regenerator can reduce the system's total exergy loss by up to 22.4% [33] and increase overall system efficiency [24].

However, while regeneration technology enhances thermodynamic performance, there remains an upper limit to the achievable heat



(a)



(b)

Fig. 1. The number of papers regarding Carnot battery on Web of Science from 2015 to 2025 (a) and the fundamental principles of Carnot battery (b).

storage temperature when the heat pump (HP) solely relies on ambient heat sources [34,35]. To overcome this constraint, the integration of external heat sources such as industrial waste heat and solar energy has emerged as a key strategy. This approach not only allows for the utilization of low-grade heat to improve overall energy efficiency but also reduces the required compressor outlet temperature when high-grade heat sources are integrated [36], thus relaxing operational demands and lowering system costs. Consequently, thermal-integrated Carnot battery, as a promising pathway toward enhanced system performance and economic viability, has been extensively investigated [29,37,38].

2.2.3. Thermal-integrated Brayton cycle

Thermal-integrated Brayton cycle-based pumped thermal energy storage (TI-BPTES) is a promising variant of B-PTES that incorporates external heat sources, including industrial waste heat, geothermal energy, or solar thermal energy, to partially replace the electrical input required to power the HP during the charging phase [36,37,39]. During charging, this integration enables either an increase in heat storage temperature at constant compressor power, or a reduction in compressor work for a given storage temperature. Two primary thermal integration strategies have been identified: low-grade heat sources preheat the working fluid via the evaporator, whereas high-grade sources directly

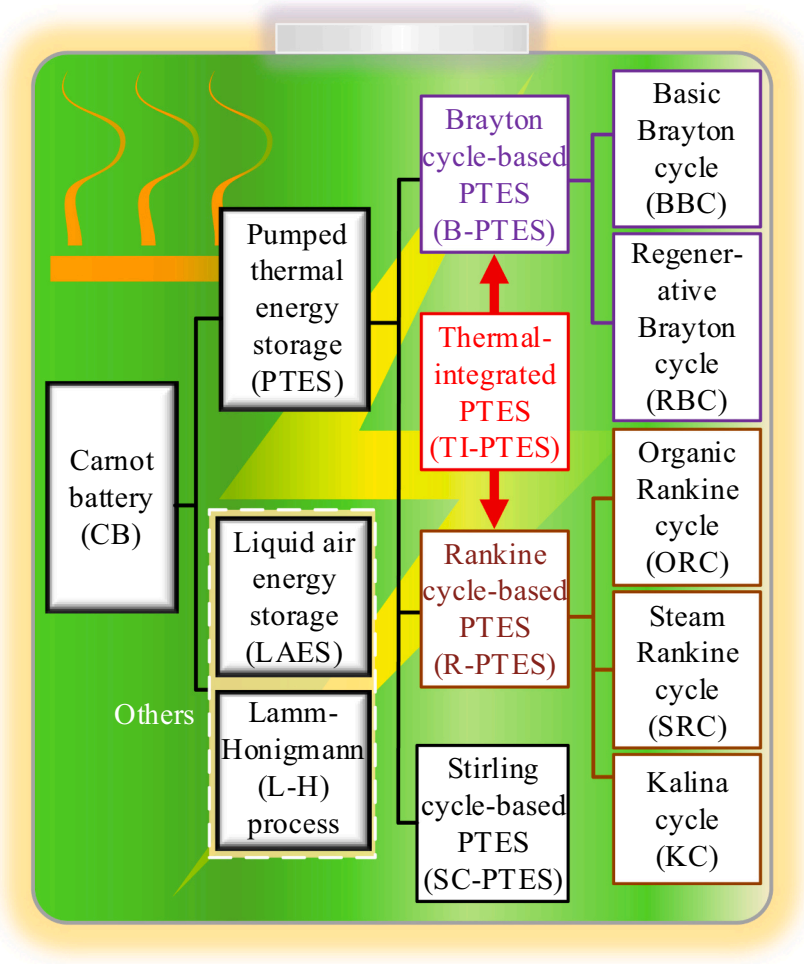


Fig. 2. Classification of Carnot battery.

supply heat to the thermal storage unit [36,37]. Moreover, Liu et al. (2025) proposed an innovative multi-temperature zone cascade cryogenic cooperative system that minimizes exergy losses during heat exchange by harnessing the cold energy of liquefied natural gas in conjunction with staged compression [32].

However, the thermal integration of current B-PTES systems is still subject to multiple constraints. When integrating low-grade heat sources, the low temperature significantly reduces the efficiency of the HP, while the limited temperature difference available for heat transfer between the heat source and working fluid restricts system performance. In the case of high-grade heat source integration, although thermodynamic efficiency can be substantially improved, the associated requirements for high-temperature-resistant materials, thermal insulation, and sealing reliability significantly increase capital cost and operational complexity [40]. Consequently, maximizing operating temperature does not necessarily result in superior techno-economic performance. Although direct injection of high-temperature heat into the hot tank appears conceptually attractive due to its simplicity and high theoretical efficiency, its practical implementation faces substantial engineering challenges, including precise temperature regulation, coordinated operation of subsystems, effective thermal management of the storage unit, and limitations under low-load operating conditions [36]. Moreover, many reported performance advantages are derived under idealized operating assumptions, whereas transient thermal losses and the dynamic interactions among coupled subsystems remain insufficiently quantified in practical scenarios.

In summary, B-PTES is evolving toward higher efficiency, lower cost, and enhanced flexibility, including multi-energy cogeneration and off-design operation capabilities [41–43]. Specifically, the regenerative system demands optimization of regenerator efficiency and improved coordination with the thermal storage subsystem to minimize thermal losses and maximize energy utilization [44]. For the thermal-integrated system, efficient integration approaches and optimal component configurations across a broad spectrum of heat source temperatures—from below 150 °C to above 300 °C—require further investigation to reduce capital expenditure [38]. Concurrently, the development of dynamic operation and control strategies that can adapt to highly variable heat source conditions is essential for successful commercial deployment [36]. The key advancement of TI-BPTES lies in its ability to diversify energy inputs, enable multi-energy synergy, and substantially improve economic performance [29].

2.3. *Rankine cycle-based Carnot battery*

Rankine cycle-based Carnot battery, also known as Rankine cycle-based pumped thermal energy storage (R-PTES), primarily uses organic fluids or water as the working fluid [45,46]. Energy conversion is achieved through the phase-change processes of liquid evaporation and vapor condensation. This system is particularly suitable for medium-to-low temperature heat storage applications (<400 °C) [23] and can be flexibly integrated with external heat sources, with its diverse configurations illustrated in Fig. 4. In the figure, the basic organic and steam Rankine cycle is represented by black process lines, while orange and red lines denote the Kalina cycle and thermal-integrated improved configurations, respectively.

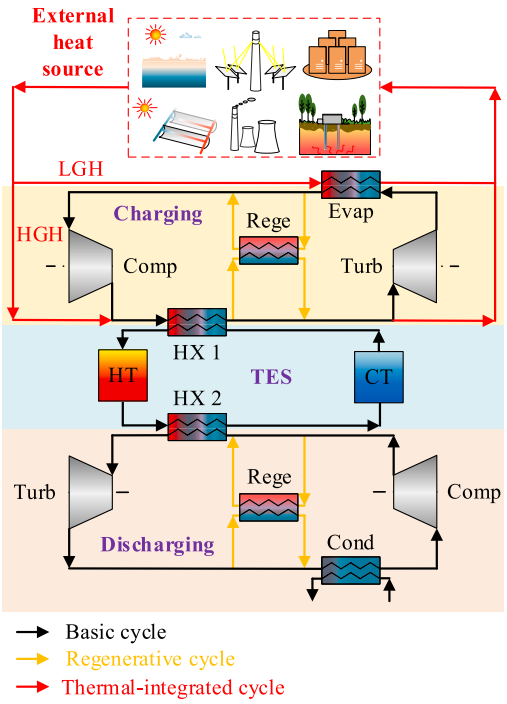


Fig. 3. Schematic diagram of Brayton Carnot battery. (Comp: Compressor. Turb: Turbine. Cond: Condenser. Evap: Evaporator. HX: Heat exchanger. Rege: Regenerator. HT: Hot tank. CT: Cold tank. HGH: High-grade heat. LGH: Low-grade heat. TES: Thermal energy storage).

2.3.1. Steam Rankine cycle

The steam Rankine cycle using water as the working fluid represents the conventional R-PTES configuration. On the charging side, an organic working fluid HP cycle is typically employed to transfer heat into the thermal storage unit, such as pressurized water or phase change materials [47–50]. During discharge, the water absorbs thermal energy to generate steam, which drives a turbine connected to a generator for electricity production [51,52]. Conventional enhancements such as regenerative and reheat configurations are not discussed in detail here.

This technology benefits from technical maturity and an environmentally benign working fluid. However, water exhibits low vapor pressure and a large specific volume at medium-to-low temperatures, which limits the system's energy density and leads to degraded performance under partial-load conditions. Consequently, organic working fluids are increasingly favored in Rankine cycle-based Carnot battery. Due to the strong match in research focus and system architecture between the organic Rankine cycle (ORC) and thermal-integrated Carnot battery [19,53–58], these two systems will be jointly analyzed in the following section.

Where energy density (ρ_e) is a critical parameter influencing the scale and cost of a Carnot battery. It is defined as the ratio of the electrical energy output during a complete charge-discharge cycle to the volume of the thermal energy storage tank(s) [59–62]:

$$\rho_e = \frac{E_{out}}{V_{tank}} \tag{1}$$

where V_{tank} denotes the total volume of the storage tank(s) [59,62]. A higher energy density implies a more compact system, greater flexibility in site selection, and reduced investment costs for a given capacity.

2.3.2. Organic Rankine cycle and thermal-integrated Rankine cycle

To overcome the limitations of water as a working fluid, the ORC Carnot battery, utilizing low-boiling-point organic fluids such as R245fa and R1233zd(E), has become the most extensively studied configuration of R-PTES. This system operates efficiently at low temperatures, is well suited for integrating low-grade waste heat in the range of 80–150 °C, and significantly reduces operating pressure [53,63,64].

Thermal-integrated Rankine cycle-based pumped thermal energy storage (TI-RPTES) commonly adopts a combined HP and ORC configuration, which significantly improves system performance by integrating external heat sources [51,52,65–67]. This design enables component sharing and can even incorporate reversible machinery to enhance operational flexibility [68,69]. Moreover, when the heat source temperature exceeds 90 °C, TI-RPTES typically achieves higher efficiency and a lower cost compared to non-integrated systems [20,47].

In addition, although the organic flash cycle has been proposed as an alternative for applications requiring large thermal storage temperature differences [70] and shows certain efficiency advantages under high-temperature-difference and part-load conditions [71], comprehensive system-level comparative studies indicate that basic ORC-based systems outperform organic flash cycle-based configurations in both thermodynamic performance and economic viability [19,56]. Consequently, the ORC remains the most technically and economically competitive option for the discharge side of R-PTES systems to date.

2.3.3. Kalina cycle

Kalina cycle (KC) is a variant of the Rankine cycle. Which commonly employs non-azeotropic binary mixtures, such as ammonia-water [72,73], and leverages their temperature glide during evaporation to achieve improved thermal matching with variable-temperature heat sources, thereby minimizing irreversible heat transfer losses [74,75].

The enhancement of heat transfer process efficiency allows KC to achieve higher overall thermal efficiency than ORC under identical temperature constraints [76]. However, studies indicate that even with the use of improved alcohol-based working fluids, the second law efficiency of KC remains lower than that of ORC systems at the same

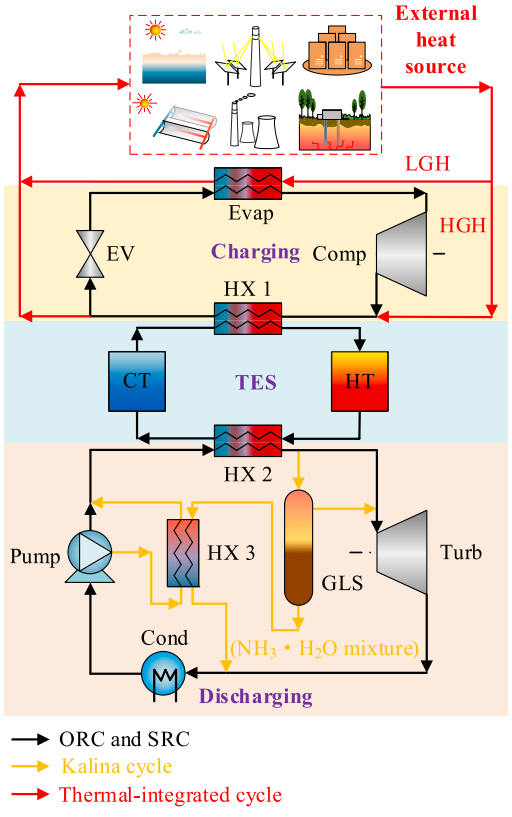


Fig. 4. Schematic diagram of Rankine Carnot battery. (Comp: Compressor. Turb: Turbine. Cond: Condenser. Evap: Evaporator. HX: Heat exchanger. HT: Hot tank. CT: Cold tank. HGH: High-grade heat. LGH: Low-grade heat. GLS: Gas-liquid separator. EV: Expansion valve. TES: Thermal energy storage).

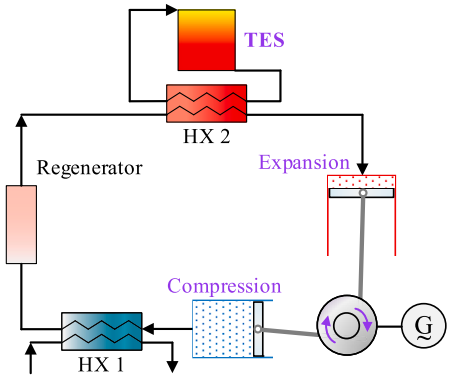


Fig. 5. Schematic diagram of a Stirling cycle-based Carnot battery.

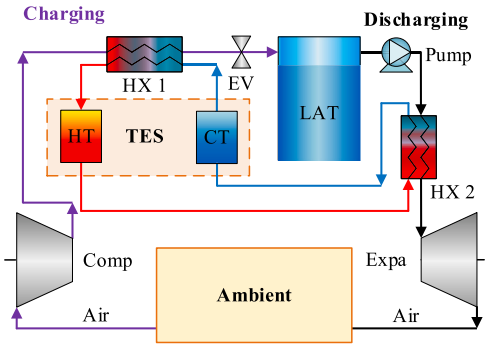


Fig. 6. Schematic diagram of liquid air energy storage. (Comp: Compressor. Expa: Expander. HX: Heat exchanger. HT: Hot tank. CT: Cold tank. LAT: Liquid air tank. EV: Expansion valve. TES: Thermal energy storage).

temperature range [77]. This apparent discrepancy may stem from the fact that compared to ORC, the KC demonstrates comparatively greater advantages in medium-to-low temperature heat sources and small-scale power systems [78,79].

The KC enables working fluid concentration adjustment through processes including gas-liquid separation. However, this requires auxiliary components such as fractionator and absorbers, leading to significantly greater system complexity and higher capital, operational, and maintenance costs compared to the conventional Rankine cycle [72].

In summary, R-PTES offers a well-defined technical pathway for medium-to-low temperature energy storage applications. The SRC configuration is particularly suitable for retrofitting existing power plants [51,80,81], whereas ORC systems and their thermal-integrated variants have emerged as the mainstream solution owing to a favorable balance between thermodynamic performance, system flexibility, and engineering feasibility. The KC is more suitable for medium-to-low temperature and small-power systems, while the organic flash cycle requires further experimental validation and performance assessment.

2.4. Stirling cycle-based Carnot battery

Stirling cycle-based Carnot battery is namely Stirling cycle-based pumped thermal energy storage (SC-PTES). Fig. 5 shows the operating principle of the Stirling cycle-based Carnot battery in the discharging process, while the charging process follows the reverse thermodynamic pathway. A regenerator is positioned between the hot and cold cylinders to improve thermal efficiency, and the working fluid undergoes periodic compression and expansion during operation. The Stirling engine works as a heat engine, converting stored thermal energy into electricity while rejecting waste heat through the cold-side heat exchanger.

SC-PTES employs the concept of single-machine bidirectional operation, whereby the same mechanical system functions as a HP during charging and as a heat engine during discharging, resulting in a compact design [82]. Nilsson's research demonstrates the feasibility of SC-PTES, showing that the overall system efficiency is considerable when high-temperature fluids are utilized [82]. Moreover, energy storage is optimal only on the high-temperature side. Owing to the structural advantages inherent in Stirling cycle heat engines, several experimental studies have been conducted on their integration with solar thermal energy [83–86]. These investigations have driven key technological breakthroughs in critical areas including heat storage material compatibility, enhancement of thermodynamic performance, system integration design, and commercial-scale economic evaluation. However, this technology remains in the early stages of development, and the reliability and cost-effectiveness of large-scale deployment continue to pose significant challenges.

2.5. Other configurations

Among Carnot battery configurations, liquid air energy storage and the Lamm–Honigmann process exhibit distinct thermodynamic characteristics compared with conventional Brayton- and Rankine-based systems. Therefore, this paper classifies them as separate configurations, and this section introduces their technical features and development status.

2.5.1. Liquid air energy storage

Liquid air energy storage (LAES), characterized by its power-to-cold-to-power conversion mechanism, represents a distinct form of Carnot battery that employs liquid air as the medium for cold energy storage

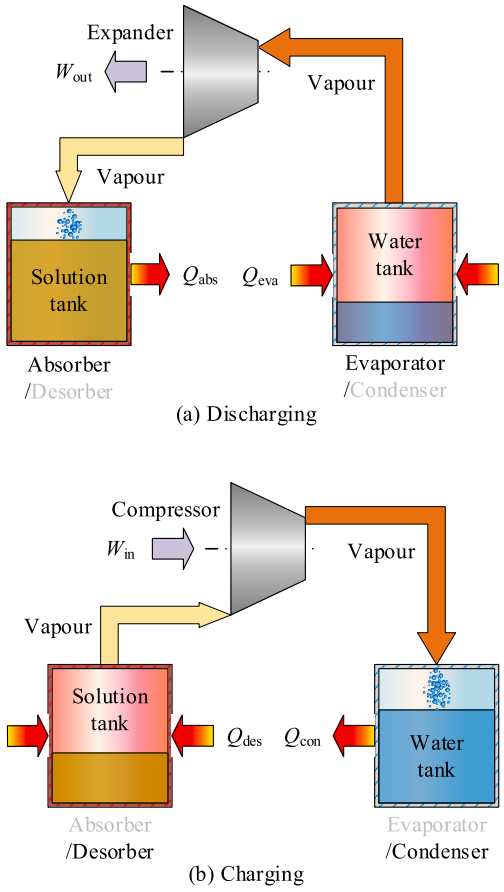


Fig. 7. Schematic diagram of the Lammn-Honigmann process: (a) the process of discharging; (b) the process of charging.

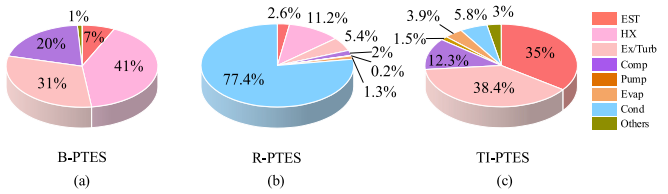


Fig. 8. Exergy destruction in Carnot battery of (a) B-PTES [102], (b) R-PTES [103] and (c) TI-PTES [104].

[14,18]. As shown in Fig. 6, during the charging process, ambient air is compressed and subsequently liquefied, while the associated compression heat is captured and stored. In the discharging phase, the stored thermal energy, either supplemented by or replaced with an external heat source, is used to vaporize the liquid air, which then expands through a turbine to generate electricity [87–89].

The primary advantage of LAES resides in its exceptionally high energy density and compact system footprint [14,90]. By implementing strategies such as efficient recovery of compression heat and integration of liquefied natural gas cold energy, the system performance can be substantially improved [88]. The hybrid configuration combining LAES with PTES, known as PTLAES, is capable of achieving simultaneously high efficiency and high energy density [91–93]. Moreover, the integration of LAES with nuclear power plants further underscores its potential, demonstrating an overall system efficiency of 51% and an energy density of 116 kWh/m^3 [94].

In summary, LAES represents a distinctive Carnot battery pathway for grid-scale long-duration energy storage owing to its high energy density and compact footprint. Current research primarily focuses on improving the efficiency of liquefaction and cold energy recovery processes, while advancing integration with external heat or cold energy sources to further enhance system performance and economic viability [95–98]. However, the relatively high energy consumption of cryogenic processes and system complexity remain important challenges for further commercialization.

2.5.2. *Lamm-Honigmann process thermochemical energy storage*

This technology stores energy through reversible chemical adsorption and desorption reactions [99], utilizing working pairs such as LiBr/H_2O, zeolite/H_2O, or H_2O/NH_3. The fundamental principle is illustrated in Fig. 7. During the discharge phase (absorption process), the evaporation heat (Q_{eva}) causes water in the evaporator to vaporize. The resulting steam drives an expander to perform mechanical work and subsequently enters the absorber. The substantial absorption heat (Q_{abs}) released during this process can be recovered and utilized in the evaporator to generate additional steam [100,101]. During the charging phase (desorption process), desorption heat (Q_{des}) is supplied to separate the working pairs in the desorber. Electrical energy drives the compressor to perform work, and the compressed steam then enters the condenser to release condensation heat (Q_{con}). This recovered heat (Q_{con}) can be used to support the desorption process, thereby establishing a concentration gradient for energy storage.

The advantages of this technology include its high energy density, operation near-ambient temperature, and low self-discharge rate [100]. When the H_2O/NH_3 working pair is used, the system can achieve a better performance. Moreover, its efficiency approaches the Carnot limit under near-ambient temperature operation [100]. Despite its significant potential for long-duration energy storage, research in this area remains limited to date. The primary challenges focus on the optimization of working pairs, improvement of dynamic response, and the structural design of reactors and heat exchangers [101].

2.6. *Summary of Carnot battery configurations*

Carnot battery has evolved into a diversified technology landscape. B-PTES dominates high-temperature energy storage applications due to its inherent high-temperature capability, while R-PTES serves medium-to-low temperature scenarios with its maturity and operational flexibility. LAES and PTES also provide economically viable technical pathways for repurposing aging power plants into large-scale energy storage facilities. Meanwhile, benefiting from its compact structure, SC-PTES has attracted significant attention for small-scale distributed energy storage applications. Lamm-Honigmann process thermochemical energy storage has the advantages of near-ambient temperature and low self-discharge rate, but currently only very limited research has been conducted on it.

The evolution of Carnot battery configurations reveals a clear transition from generalized standalone cycles toward application-oriented thermal integration. Early milestone studies established systematic thermodynamic and loss-analysis frameworks for PTES [61,62], laying the foundation for reproducible comparisons among different configurations. These early studies focused on generic cycle architectures and did not consider interactions with external thermal environments, which is the focus of the present work.

A key advance was the unified framework of Carnot battery proposed by Dumont et al. [18], which enabled systematic comparison among previously fragmented technological pathways. More importantly, recent configuration innovation suggests an emerging trend: rather than relying solely on internal cycle refinement, new architectures increasingly improve system feasibility through deeper utilization of external thermal resources and existing infrastructures. Representative examples include liquefied natural gas cold-energy-assisted multi-temperature systems [32] and thermal-integrated coal-fired power plant concepts [51], both of which demonstrate how thermal coupling can reshape conventional Carnot battery configurations. Compared with isolated systems, thermal-integrated systems appear particularly promising because they enable more effective utilization existing thermal assets.

However, current progress also indicates that the benefits of thermal integration are strongly dependent on site-specific thermal conditions and infrastructure compatibility. Therefore, a key challenge for future configuration development is not merely proposing new architectures, but identifying scenarios in which thermal-integrated Carnot batteries can achieve practical advantages over standalone systems.

3. Key components of Carnot battery

The performance of a Carnot battery is dependent on the synergistic coordination of its key components. Consequently, targeted component-level research is essential to achieve overall system performance improvement and cost reductions, enabling systematic identification and exploitation of optimization potential. Fig. 8 presents the exergy destruction across the full charge–discharge cycle of three Carnot battery configurations, including B-PTES [102], R-PTES [103], and TI-PTES [104]. Turbomachinery, heat exchangers, and thermal energy storage (TES) system account for the majority of the total system exergy destruction. Consequently, further improvements in system performance are fundamentally constrained by losses in these units, making their optimization the most promising pathway toward substantial performance enhancement.

3.1. *Compressors and expanders*

The current technical development primarily focuses on the selection and optimization of turbomachinery and positive displacement machinery. Turbomachinery (e.g., axial-flow compressors and turbines), as the mainstream solution, is well suited for high-power and high-flow-rate applications. Its isentropic efficiency typically ranges from 80% to 90%, but it experiences efficiency degradation under off-design operating conditions [105]. In contrast, positive displacement machinery (e.g., reciprocating and screw types) exhibits superior performance in small-scale, high-pressure-ratio systems, with enhanced adaptability under part-load conditions [105]. Among these, screw-type machines

Table 1
Information on the thermal energy storage medium of Carnot battery.

Type	Medium	Temperature range [K]	Function	Configuration	Ref.
Sensible heat	Al_2O_3	293–1200	heat / cold	B-PTES	[128]
	TiO_2	343–1323	heat / cold	B-PTES	[129]
	Concrete	343–1323	heat / cold	B-PTES	[129]
	Limestone	343–1323	heat / cold	B-PTES	[129]
	Masonry	343–1323	heat / cold	B-PTES	[129]
	Granite pebble	171–1000	heat / cold	B-PTES	[36]
	Gravel / Quartz	113–1246	cold	B-PTES	[32]
	Magnesia brick	73–1533	heat	B-PTES	[32]
	Magnetite	550–850	heat	B-PTES	[130]
	Silicon-based particles	228–1400	heat / cold	B-PTES	[131]
	Solar salt (60% $NaNO_3$ + 40% KNO_3)	493–873	heat	B-PTES	[28,102]
	HITEC XL	403–823	heat	B-PTES, R-PTES	[132]
	Quaternary molten salt	460–920	heat	B-PTES	[25]
	Therminol 66	264–616	heat	B-PTES	[102]
	Therminol VP-1	403–443	heat	R-PTES	[116]
	Synthetic oil	233–573	heat	B-PTES	[32]
	Pressurized water	323–423	heat	R-PTES	[48,70,133]
	Methanol	175–338	cold	B-PTES	[134]
	Water-glycol mixture	233	cold	R-PTES	[135]
	Butane	135	cold	B-PTES	[102]
Latent heat	KNO_3-$LiNO_3$ eutectic mixture	405	heat	R-PTES	[45]
	$LiNO_3$-$NaNO_3$-KNO_3 (30–18-52%)	396	heat	R-PTES	[66]
	NaOH powder	591	heat	B-PTES	[33]
	$CaCl_2$ aqueous solution	218	cold	B-PTES	[33]
	Eutectic aqueous salt solution (22.4% NaCl + H_2O)	251.8	cold	B-PTES	[28]
	Paraffin wax	358–418	heat	R-PTES	[121]
	Polyethylene wax / expanded graphite composite PCM	386–394	heat	–	[136]
	Erythritol	363–413	heat	–	[122]
	High-density polyethylene	393–433	heat	R-PTES	[27]
	Ice	273	cold	R-PTES	[137]
Thermochemical	$Ca(OH)_2$ / CaO	667–884	heat	B-PTES	[126]
	MgO / $Mg(OH)_2$	398–623	heat	R-PTES	[75]
	Methanol	473–623	heat	B-PTES	[138]
	$CaCl_2$-H_2O solution	313–391.7	heat	R-PTES	[127]

are particularly favored in ORC systems due to their capability to handle two-phase flow and high operational reliability [106]. Nevertheless, no universal solution currently exists, as machinery selection remains highly dependent on system scale, operating pressure ratio, working fluid properties, and off-design performance requirements.

Reversible design, as a key research direction, can effectively reduce system complexity and initial investment by enabling the compression and expansion functions of the charging and discharging processes within a single device. Steger et al. (2022) demonstrated that by optimizing the high-pressure side opening angle to approximately −155°, a combined efficiency of 75% could be achieved, with estimated overall system efficiency reaching 66% [69]. However, an efficiency gap of about 7 percentage points persisted compared to dedicated components. An experimental study by Weitzer et al. (2025) further validated the feasibility of a reversible HP-ORC system [107]. However, it also revealed that system performance is primarily constrained by the screw machine's efficiency in its two operating modes: up to 78% in compressor mode and 60% in expander mode. This indicates substantial potential for further optimization.

More fundamentally, reversible machinery introduces an inherent trade-off between structural simplification and thermodynamic performance. While integrating compression and expansion functions within a single device can reduce system complexity and investment requirements, the resulting performance penalty remains a major obstacle to practical deployment, particularly under off-design conditions.

3.2. Heat exchanger

As the key component governing thermal energy exchange in a Carnot battery, the heat exchanger accounts for a substantial portion of total system exergy destruction [48,108], thereby exerting a dominant influence on overall thermodynamic irreversibility. High-temperature heat exchangers must withstand temperatures exceeding 500 °C, posing significant challenges to material thermal stability and mechanical strength [59]. Low-temperature heat exchangers are required to operate stably in environments below −50 °C, where sealing performance and material brittleness at low temperatures become critical design considerations [33]. To enhance heat transfer efficiency and reduce system volume, compact and high-efficiency heat exchange technologies, such as plate-fin heat exchangers and multi-stream plate-fin heat exchangers, have been widely studied and implemented. Among these, multi-stream plate-fin heat exchanger design significantly affects the performance of helium-based PTES systems [93]. Moreover, advances in reversible heat exchanger technology are a critical enabler for the realization of reversible HP-ORC systems, thereby offering a viable pathway to substantially reduce the total investment cost of Carnot battery [109].

Beyond enhancing heat exchanger efficiency, improving temperature matching between hot and cold streams through strategies such as staged condensation and staged evaporation represents a highly effective approach to elevating overall system performance. These techniques align the temperature profiles of the heat transfer medium and working fluid across the exchanger, thereby minimizing thermodynamic irreversibility associated with finite-temperature driving forces and yielding measurable gains in cycle efficiency [110]. Moreover, Yang et al. (2025) significantly increased the evaporator inlet temperature by integrating a supercritical extraction, compression, and reheating process. This improvement in temperature matching enabled the system to achieve a higher system efficiency even with a waste heat source at only 86.4 °C [52]. However, excessive pursuit of improved temperature matching often requires larger heat transfer areas and more complex exchanger configurations, which may increase manufacturing difficulty and system complexity.

In summary, heat exchanger optimization represents a critical yet inherently constrained pathway for Carnot battery improvement. While enhanced heat transfer and temperature matching can effectively reduce exergy destruction, practical implementation remains bounded by material limitations, exchanger complexity, and operational constraints.

3.3. Thermal energy storage unit

The thermal energy storage type, material selection, and tank arrangement are key factors for TES unit, greatly impacting the system performance, cost, energy density, and operational flexibility of Carnot battery.

Sensible heat energy storage stores energy by increasing the temperature of the storage medium and is currently the most mature and widely adopted thermal storage technology. Commonly used media include: (a) Solid packed beds (e.g., rock or ceramic pebbles), which offer advantages such as low cost, high temperature resistance (>1000 °C), and chemical inertness, making them suitable for Brayton cycle systems [111,112]. (b) Molten salts, which possess a relatively high specific heat capacity and operate over a wide temperature range (approximately 230–560 °C), are the preferred medium for medium-to-high temperature applications [113–115]. (c) Thermal oils (e.g., Therminol series), suitable for medium-to-low temperature ranges (120–150 °C), are commonly employed in ORC systems [103,116,117]. (d) Pressurized water, characterized by low cost, high availability, and high thermal capacity, typically operates within a temperature range of 60–150 °C and is the most widely used medium in Rankine-type Carnot battery [48,71,118]. In terms of energy density, rock-filled beds can achieve values of 50–100 kWh/m^3, while molten salts typically range from 15 to 30 kWh/m^3. However, the latter exhibits superior heat exchange performance [91,111,119].

Latent heat energy storage utilizes the latent heat of phase change in phase change materials (PCMs) to store energy, offering advantages such as high energy density and nearly isothermal charging and discharging characteristics [120]. Based on operating temperature, PCMs can be classified into two categories: medium-to-low temperature PCMs (e.g., paraffins, hydrated salts; <200 °C) and high-temperature PCMs (e.g., nitrates, metals; >300 °C) [28,121–123]. Their energy density can exceed 200 kWh/m^3, making them suitable for a wide range of Carnot battery. To further enhance performance, cascaded latent heat storage technology employs multiple PCMs with different phase change temperatures in combination. By optimizing temperature matching, it effectively reduces exergy destruction [124]. Studies show that a three-stage cascaded latent heat storage system can achieve an overall system efficiency of 100.1% and an exergy efficiency of 59.7%, representing improvements of 27.9 and 14.0 percentage points, respectively, over single-stage systems [121]. The successful application of this technology requires coordinated matching between the working fluid and the melting points of the PCMs [121,125].

Thermochemical energy storage stores energy through reversible chemical reactions. Common storage media include $Ca(OH)_2/CaO$ and $LiBr/H_2O$, offering an energy density of approximately 30 kWh/m^3. Thermochemical energy storage is compatible with thermodynamic cycles such as the Kalina cycle, Brayton cycle, and Lamm-Honigmann process [75,100,126,127]. The specific information of commonly used thermal storage media is summarized in Table 1 [25,27,28,32,33,36,45,48,66,70,75,102,116,121,122,126–138].

The main types of tank arrangement in a TES unit include single-tank, double-tank, and multi-tank. Currently, the double-tank system (with separate cold and heat storage) has become the mainstream solution due to advantages such as fluid isolation, simple control, and avoidance of mixing losses. The single-tank system, which primarily employs thermal stratification technology, features a simple structure and low cost. However, it is susceptible to thermal mixing losses and temperature glide effects, limiting its application to experimental setups or specific scenarios [104,107]. Multi-tank systems, by contrast, are suitable for complex applications and can improve overall energy efficiency and operational flexibility through multi-temperature zone designs or integration of different-grade heat sources [110,139]. The selection of an actual configuration requires a comprehensive trade-off among efficiency, energy density, system complexity, and cost.

3.4. Summary of key components

Progress in key components of Carnot battery suggest that reversible operation is emerging as a promising, yet still exploratory, design direction for power machinery and heat exchangers. Experimental verification of a bidirectional screw machine demonstrated the feasibility of operating the same unit in both HP and ORC modes, providing a practical pathway to reduce the cost associated with dedicated compression and expansion equipment [107]. Likewise, thermal imaging experiments combined with analytical modeling revealed the fundamental difference in heat flux density of a reversible heat exchanger under condensation and evaporation modes, providing the first experimental evidence for bidirectional matching design [109].

However, these studies simultaneously expose a common challenge of reversible components: a single device optimized for bidirectional operation may struggle to maintain thermodynamic optimality in both modes. For example, the reversible screw machine exhibited restricted temperature lift and substantially lower expansion efficiency than dedicated expanders [107], whereas satisfying extremely small pinch-point requirements under reversible operation may introduce heat transfer area redundancy exceeding 46% [109]. Furthermore, although advanced modeling approaches, such as the adaptive segmented temperature transfer matrix, improve the prediction accuracy of multi-stream heat exchangers under variable thermophysical properties, their reliance on empirical correlations and lack of experimental validation still limit practical design guidance [93].

For TES units, current development mainly involves balancing energy density, thermal losses, and system complexity through the selection of storage media and tank arrangements. In this context, recent exploratory studies have introduced novel storage configurations or media to address specific thermodynamic constraints. Cascaded latent heat storage was proposed to alleviate overcharging and improve temperature matching between thermal storage materials and the working fluid in Carnot batteries [121], while ice-slurry cold storage demonstrated the potential of phase-change media to reduce cold loss through efficient thermal matching with the working fluid [139]. However, these studies remain highly case-specific and still rely on numerical assumptions, auxiliary systems, or unverified operational stability, which may limit their broader engineering applicability.

4. Analysis of system performance and economy

The commercial deployment of Carnot battery depends on its integrated technical and economic performance. This section conducts a sensitivity analysis of system performance and economic. The key design and operational parameters are discussed, including system configuration, system parameters, isentropic efficiency of turbomachinery, heat exchanger parameters, and heat storage temperature on round-trip efficiency (RTE) and levelized cost of storage (LCOS) of Carnot battery. This section aims to establish a comprehensive, multi-dimensional foundation for informed engineering deployment decisions.

4.1. Key technological and economic indicators

To quantitatively evaluate both the technical performance and economic viability of Carnot battery, this paper introduces two key metrics: RTE as a technical performance indicator and LCOS as an economic metric, both of which are rigorously defined and derived step by step.

4.1.1. Technological assessment model

The theoretical foundation of Carnot battery originates from the Carnot cycle. Carnot battery consists of three core processes: charging, thermal energy storage, and discharging. During the discharge phase, an ideal heat engine operating between a high-temperature reservoir (T_1) and a low-temperature reservoir (T_2) achieves the maximum thermal-to-work conversion efficiency, known as the Carnot efficiency:

$$\eta_{c,HE} = \frac{W_{out}}{Q_{st,HE}} = 1 - \frac{T_2}{T_1} \tag{2}$$

Where W_{out} denotes the net power output from the heat engine and $Q_{st,HE}$ represents the heat absorbed by the heat engine from the hot tank of TES unit.

During the charge phase, the coefficient of performance (COP) of an ideal HP operating on a reverse Carnot cycle between the same two temperatures is given by:

$$COP_{c,HP} = \frac{Q_{st,HP}}{W_{in}} = \frac{T_1}{T_1 - T_2} \tag{3}$$

Where W_{in} denotes the net power input to the HP and $Q_{st,HP}$ represents the heat rejected by the HP to the hot tank of TES unit.

The thermal storage efficiency (η_{st}) is defined as the ratio of the heat output to the heat input of the thermal energy storage unit over one charge and discharge cycle [140,141]:

$$\eta_{st} = \frac{Q_{st,HE}}{Q_{st,HP}} \tag{4}$$

Its value typically approaches unity [23,142].

Therefore, RTE (η_{rt}) can be expressed and is conventionally defined as the ratio of the electrical energy output by the system to the electrical energy consumed [71,143]:

$$\eta_{rt} = \frac{E_{out}}{E_{in}} = \frac{\eta_{HE} \cdot Q_{st,HE}}{Q_{st,HP}/COP_{HP}} = COP_{HP} \cdot \eta_{st} \cdot \eta_{HE} \tag{5}$$

Where η_{HE} denotes the heat engine efficiency. Correspondingly, the RTE can also be expressed as the ratio of net power output to net power input [130,144,145]:

$$\eta_{rt} = \frac{W_{out}}{W_{in}} \tag{6}$$

Moreover, assuming perfect thermal storage efficiency ($\eta_{st} = 1$) [70,71], ideal RTE is given by the product of the charging COP and the discharging efficiency [146]:

$$\eta_{rt,idea} = COP_{c,HP} \cdot \eta_{c,HE} = \left(\frac{T_1}{T_1 - T_2}\right) \cdot \left(1 - \frac{T_2}{T_1}\right) \tag{7}$$

This result establishes the theoretical RTE limit of 100%.

However, this limit cannot be reached in engineering practice because the performance of actual systems is constrained by multiple irreversible losses. Specifically, the irreversibility of turbomachinery [62], finite temperature difference in heat transfer [59,129,146,147], and thermal loss [148] each significantly degrade overall system performance.

Notably, when integrating external heat sources such as industrial waste heat, the coefficient of performance of the HP can significantly exceed 1 [49,142,146], indicating a substantial increase in the heat input to the hot tank ($Q_{st,HP}$) during the charging phase. Consequently, the net power output by the system during discharging (W_{out}) may greatly surpass the net power input during charging (W_{in}). From a grid-level perspective, evaluated on an electricity-to-electricity basis, this results in an RTE exceeding 100% [149]. This does not violate the law of conservation of energy because the additional energy is supplied by external heat sources.

RTE reflects the overall efficiency of the three core processes of Carnot battery, including charging, energy storage and discharging. Therefore, this paper selects RTE to evaluate the performance of Carnot battery.

Table 2
Economic models of main components of Carnot battery [20].

Component	Economic model	Applicable range
Turbine	$\log_{10}C^0_{turb} = a + b \times \log_{10}W + c \times (\log_{10}W)^2$	100–4000 kW
Compressor	$C^0_{comp} = 98400 \times (W_{comp}/250)^{0.46}$	250–10,000 kW
Pump	$C^0_{pump} = 9840 \times (W_{pump}/4)^{0.55}$	4–700 kW
Heat exchanger	$\log_{10}C^0_{hx} = a + b \times \log_{10}A + c \times (\log_{10}A)^2$	10–1000 m^2
Storage tank	$C^0_{tank} = a + b \times V_{sto} + c \times (V_{sto})^2$	$\leq$ 10,000 m^3
Generator	$C^0_{gen} = 2 \times 10^5 \times (W_{gen}/500)^{0.67}$	–

Table 3
The relevant correction factors of economic models [20].

Component	a	b	c	f_1	f_2	f_3
Turbine	2.7051	1.4398	−0.1776	0	0	3.4
Compressor	–	–	–	f_T	f_p	0.6
Pump	–	–	–	f_T	f_p	0.6
Heat exchanger	4.3247	−0.3030	0.1634	1.35	f_{p0}	1.89
Storage tank	50,990	37.04	−0.0003	1.52	0	1.49
Generator	–	–	–	0	0	0

4.1.2. Economic assessment model

The economic viability of Carnot battery is primarily assessed using the LCOS as the key metric, defined as the ratio of the total lifecycle cost to the total discharged energy over its operational lifetime [20,150,151]:

$$LCOS = \frac{C_{inv} + \sum_{i=1}^{LT} \frac{C_{ann}}{(1+r)^i}}{\sum_{i=1}^{LT} \frac{E_{gen}}{(1+r)^i}} \tag{8}$$

Where C_{inv} denotes the total investment cost of Carnot battery; C_{ann} represents the annual operation and maintenance cost; LT refers to the system lifetime, typically assumed to be 25 years; E_{gen} signifies the total annual discharged energy; and r is the discount rate, set at 5%.

$$C_{ann} = C_{OM} + C_{ele} \cdot E_{in} - R \tag{9}$$

Among them, C_{OM} is the operation and maintenance cost, assumed as 1.5% of the C_{inv}; R represents the recovery value, which is set to 0 at the end of the system lifetime; C_{ele} is the electricity price, assumed as 0.05 $/kWh.

The total investment cost of Carnot battery (C_{inv}) is dominated by turbines, compressors, pumps, heat exchangers, storage tanks, and generators. The bare cost model and its applicability are summarized in Table 2 [20]. Component costs are estimated based on key sizing parameters, including the rated power of turbomachinery (turbines, compressors, and pumps), the heat exchange area, and the storage tank capacity. The heat exchange area is derived from the thermal load and the pinch point temperature difference.

Bare costs are then adjusted using correction factors that account for operating temperature, pressure, and material selection. The detailed calculation procedure is presented in Eq. (10) [152]. The values of the relevant correction factors are summarized in Table 3 [20].

$$C_X = (f_1 \times f_2 + f_3) \times C^0_X \tag{10}$$

For operating pressures above 5 bar, the pressure correction factor (f_{p0}) for the heat exchanger is obtained from:

$$\log_{10}f_{p0} = 0.03881 - 0.11272 \times \log_{10}p + 0.08183 \times (\log_{10}p)^2 \tag{11}$$

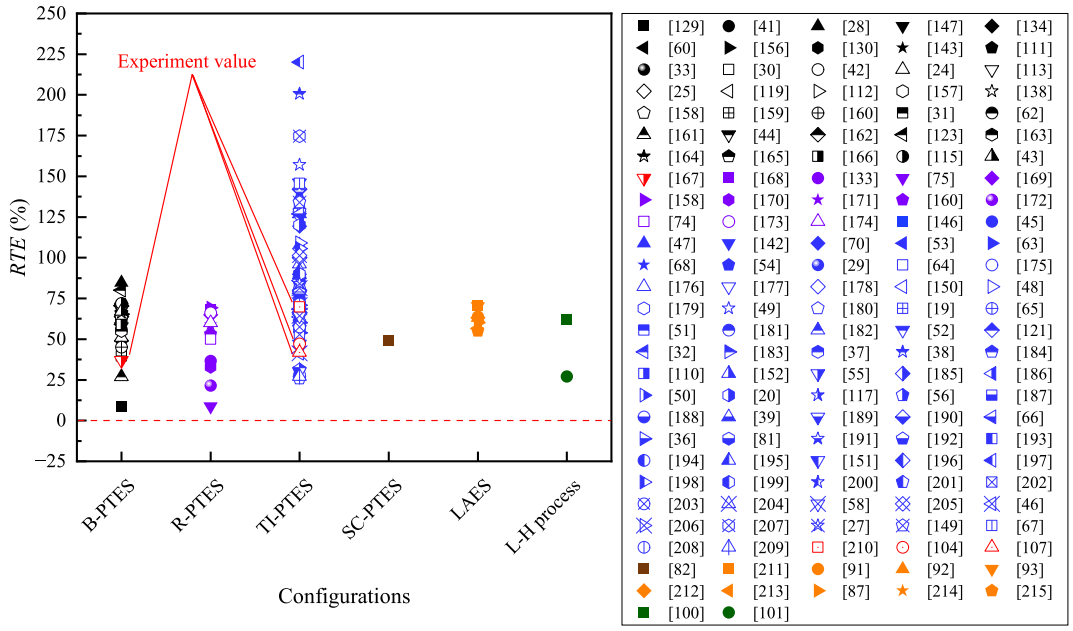


Fig. 9. Effect of configurations on round-trip efficiencies (RTE) (TI-PTES includes TI-BPTES and TI-RPTES). Data source: [19,20,24,25,27–33,36–39,41–56,58,60,62–68,70,74,75,81,82,87,91–93,100,101,104,107,110–113,115,117,119,121,123,129,130,133,134,138,142,143,146,147,149–152,156–215].

For compressors and pumps, the pressure correction factor f_p is derived from Smith function [153]. As pressure increases from 7 bar to 50 bar, f_p rises by 0.5; similarly, f_T increases by 0.6 over a temperature rise from 273.15 K to 573.15 K. Linear interpolation is applied for intermediate conditions.

When the required power or heat exchanger area exceeds the applicable range of a single unit, multiple identical pieces of equipment are employed in parallel to avoid excessive estimation errors. The total investment cost is then aggregated from all components. All cost estimates are adjusted to the reference 2019 using the CEPCI value of 607.5 [154].

$$C_{\text{inv}} = \sum C_X \times CEPCI_{2019} \Big/ CEPCI_{2001} \tag{12}$$

The LCOS is adopted as the key economic metric in this paper because it satisfies several fundamental criteria for a robust and transparent storage technology assessment [155]. As demonstrated in Eqs. (8) and (9), its formulation is simple, transparent, and based on readily available input data such as investment cost, lifetime, discount rate, and electricity price. Crucially, it incorporates the time value of money through discounting, and by amortizing total lifecycle costs (including investment, operation, and end-of-life recovery) over the total discharged energy throughout the project's lifetime (typically 25 years), it provides a fair, technology-agnostic basis for comparison.

4.2. Sensitivity analysis of RTE

The performance of Carnot battery is governed by multiple factors. At the system level, RTE is critically influenced by configuration choices and design parameters. At the component level, core parameters of key components need to be focused on, including the isentropic efficiency of turbomachinery, heat transfer parameters of heat exchangers, and the heat storage temperature of the TES unit. Other parameters, including the temperature ratio and pressure ratio of turbomachinery, and the maximum temperature of the cycle, are directly or indirectly related to the core parameters of the components and thus are not discussed separately in this paper.

4.2.1. Effect of system configuration on RTE

The application prospects of Carnot batteries are very broad. They not only can efficiently absorb surplus electricity but also flexibly integrate various-grade heat sources, such as industrial waste heat and solar energy. Different configurations can be coupled to form hybrid systems, enabling complementary advantages. Fig. 9 [19,20,24,25,27–33,36–39,41–56,58,60,62–68,70,74,75,81,82,87,91–93,100,101,104,107,110–113,115,117,119,121,123,129,130,133,134,138,142,143,146,147,149–152,156–215] summarizes the maximum RTE achieved by different Carnot battery configurations in existing studies.

In 2013, White et al. proposed a comprehensive thermodynamic analysis framework for PTES, laying the foundation for the quantitative evaluation of Carnot battery performance [61]. Subsequently, Frate et al. theoretically and numerically demonstrated the feasibility of thermal integration in 2017 [146]. Owing to their ability to effectively utilize external heat sources, thermal-integrated systems generally achieve higher RTE values compared to other configurations and have thus become a primary focus of current research. As shown in Fig. 9, the use of a dual-pressure discharge cycle and extended discharge duration in a thermal-integrated system theoretically enabled an RTE of up to 220% [197]. However, the higher RTE of thermal-integrated systems is frequently achieved through increased system complexity and stronger subsystem coupling, which may introduce additional operational challenges under practical conditions. Moreover, although a large amount of RTE data for Carnot batteries is currently available, the vast majority are based on theoretical calculations or optimized values, while experimental data remain very limited [107,210].

As shown by the red data points in Fig. 9, results indicate that the RTE of practical cycles is substantially lower than the theoretical maximum. This discrepancy primarily originates from unavoidable irreversibility in practical systems, including off-design operation of turbomachinery, finite-temperature heat transfer, thermal leakage during storage, and dynamic mismatches among coupled subsystems. Moreover, many reported high RTE values are obtained under idealized operating assumptions, potentially overestimating achievable performance in real-world deployment. Therefore, beyond advancing

theoretical research through innovative methodologies, experimental validation must be systematically strengthened to bridge the gap between modeling assumptions and real-world system behavior.

4.2.2. Effect of system parameters on RTE

The key system parameters include heat source conditions (i.e., temperature and mass flow rate), installed capacity, and operational duration. Heat source conditions critically govern the performance and cost of a thermal-integrated system; installed capacity determines the maximum thermal energy that can be stored; and operational duration directly influences the system's annual utilization factor and dispatch flexibility.

Fig. 10(a) [27,55,68,142,149,188,192,198] and (b) [180,188] illustrates that existing studies have reached divergent conclusions regarding the impact of heat source temperature and mass flow rate on RTE in thermal-integrated systems, owing to varying analytical assumptions. Nevertheless, the underlying trend indicates that increasing both parameters enhances system performance. Studies based on fixed system scales consistently report an increase in RTE with rising heat source temperature [27,55,68,142,149,192,198]. This trend arises from the improved COP at higher temperatures, while the discharging-side efficiency remains largely unaffected by the charging-side heat source temperature. In contrast, research conducted under the assumption of variable power capacity reaches different conclusions [180,188]. When system scale expands proportionally with heat source conditions, both charging and discharging power increase simultaneously, thereby maintaining a stable RTE. The primary benefit lies in the reduction of the cost. Holding all other operating and design parameters constant, an increase in heat source mass flow rate enables higher thermal input to the system, thereby allowing for increased rated capacity and greater annual energy output, both of which contribute to a reduction in cost [180]. Therefore, the apparent inconsistency in reported trends does not necessarily indicate conflicting physical mechanisms, but rather reflects differences in system boundary assumptions and scaling strategies adopted in existing studies.

System installed capacity (energy storage capacity), charging duration, and annual utilization hours are extrinsic parameters, which are design and operational choices driven primarily by economic considerations rather than thermodynamic performance. Therefore, they exhibit no direct influence on RTE, which is governed solely by internal cycle physics and component efficiencies. This independence is clearly demonstrated in Fig. 11(a) [180] and (b) [65,216]. Although these parameters are frequently reported alongside performance indicators, their influence on RTE is indirect and often mediated through changes in system design and operational strategies rather than thermodynamic mechanisms.

4.2.3. Effect of turbomachinery efficiency on RTE

As shown in Fig. 12 [20,146,158,216], the system's RTE increases continuously with improvements in the isentropic efficiency of turbomachinery. Studies have demonstrated that the isentropic efficiency of compressors and expanders is among the most sensitive parameters affecting Carnot battery performance [217], and enhancing this parameter exerts a leverage effect on overall system performance [62]. Zhao et al. (2021) reported that increasing the isentropic efficiency from 85% to 95% can raise the exergy efficiency of B-PTES from 23% to 48% [102]. Ge et al. (2021) further confirmed that the same improvement can lead to an RTE increase of over 45% [28].

It should be noted that compressor power consumption decreases with increasing isentropic efficiency. Therefore, higher compressor isentropic efficiency may also lead to a reduction in system energy storage capacity under the same operating conditions, because the associated decrease in compressor power input reduces the electrical energy stored in the charging process [20,216]. This observation suggests that improvements in compressor efficiency should be evaluated not only by their contribution to RTE enhancement, but also by their influence on effective storage capacity at the system level.

4.2.4. Effect of heat exchanger parameters on RTE

The heat exchanger parameters are important for heat exchangers to reduce heat transfer irreversibility. Among them, the effect of evaporation temperature (the operating temperature of the evaporator) on RTE is shown in Fig. 13(a) [19,20,50,53,152,175,183,187,188,190,200,206,208,216]. On the one hand, increasing the evaporation temperature enhances the COP of the HP and reduces power consumption when storing a given amount of thermal energy. Simultaneously, a smaller evaporator heat transfer temperature difference decreases irreversible losses, collectively contributing to an increase in system RTE. However, increasing the evaporation temperature may also reduce the system energy storage capacity under fixed heat source and storage temperature conditions, because the improved COP decreases compressor power consumption and consequently lowers the stored energy within the system [152]. On the other hand, an increase in the evaporation temperature at the power generation side can enhance RTE and increase electricity generation [216].

Conversely, raising the condensation temperature (the operating temperature of the condenser) lowers the COP and increases the condenser heat transfer temperature difference, thereby reducing RTE

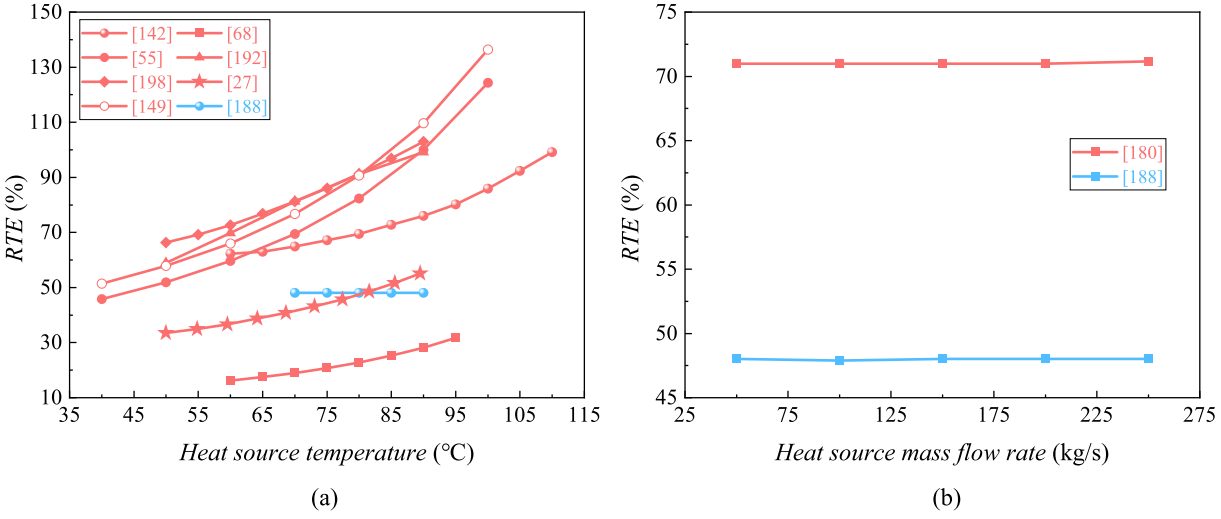


Fig. 10. Effect of heat source temperature (a) and heat source mass flow rate (b) on round-trip efficiencies (RTE) of the system under thermal integration conditions. Data source: (a) [27,55,68,142,149,188,192,198]; (b) [180,188].

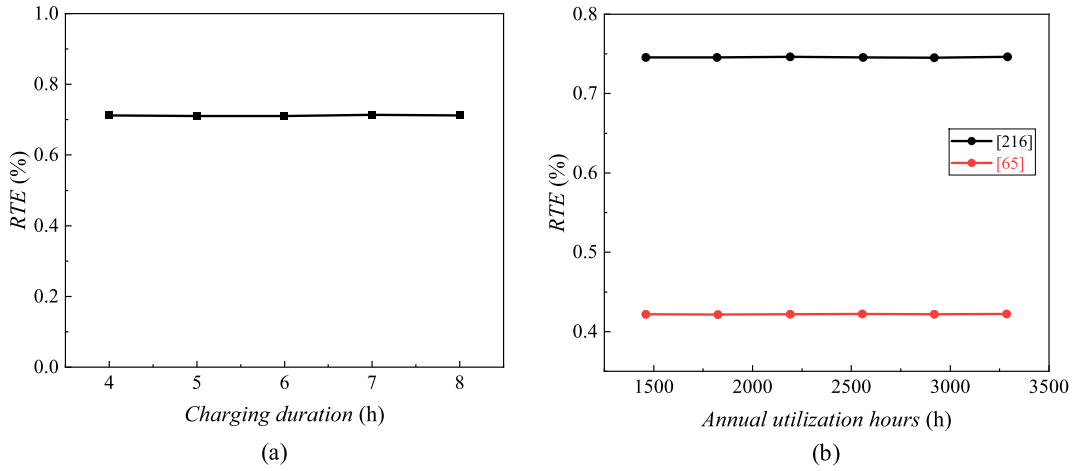


Fig. 11. Effect of the charging duration (a) and annual utilization hours (b) on round-trip efficiencies (RTE) of Carnot battery. Data source: (a) [180]; (b) [65,216].

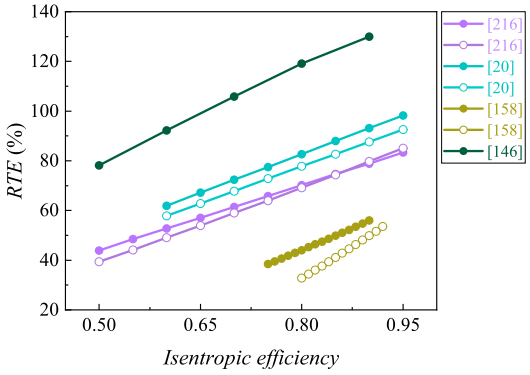


Fig. 12. Effect of isentropic efficiencies of the compressor and turbine on round-trip efficiencies (RTE) of Carnot battery. Solid circles represent the compressor curve; hollow circles represent the turbine curve. Data source: [20,146,158,216].

(see Fig. 13(b) [19,52,183]). An increase in the condensation temperature at the power generation side will reduce the efficiency at the power generation stage, thereby leading to a decrease in RTE [52].

Furthermore, the pinch point temperature difference (the minimum temperature difference between the hot and cold fluid streams within a heat exchanger) is a critical parameter for balancing heat exchanger cost and performance, and it exerts an important influence on system performance. Most studies [19,27,58,200] indicate that increasing the pinch point temperature difference reduces RTE due to heightened irreversible heat transfer losses (see Fig. 13(c) [19,27,58,180,200]).

However, Kurşun et al. (2024) observed a counterintuitive trend in their study of an integrated concentrated photovoltaic thermal system due to differences in analytical objectives [180]. To increase pinch point temperature difference, the heat transfer rate between the heat source and the working fluid must be reduced. With the heat source mass flow rate held constant, the working fluid mass flow rate during both charging and discharging cycles is consequently lowered. As a result, compressor power consumption and turbine net output power both decline. However, the net output power decreases at a slower rate than compressor power, leading to an overall improvement in RTE. This counterintuitive result highlights that the influence of pinch point temperature difference on RTE depends strongly on how the parameter is imposed within the system analysis. Under fixed system settings, increasing the pinch point temperature difference generally intensifies thermal irreversibility and lowers RTE. However, when a prescribed pinch point is maintained through adjustments in working fluid flow rate and system operation, different trends may emerge due to altered system boundary conditions and operating constraints. A smaller pinch point temperature difference improves RTE. However, heat exchanger design constraints, including finite heat transfer area, pressure drop limits and manufacturability, impose a practical lower bound, with practical designs commonly adopting values around 5 °C [218]. Within the technically feasible range, minimizing pinch point temperature difference is generally beneficial because it simultaneously mitigates heat transfer irreversibility, enhances RTE, and contributes to LCOS reduction [152].

4.2.5. *Effect of heat storage temperature on RTE*

The operating temperature range of thermal storage materials will limit the heat storage temperature (the operating temperature of the hot storage tank). Fig. 14(a) [19,20,25,27,28,33,36,37,45,47–55,58,59,62–64,66,68,74,75,81,104,107,111–114,116,119,121,125,126,129–131,133,138,143,149,151,152,157,159,161,163,167,169,170,175–177,179,180,182,186,193,194,197,204,205,207–210] illustrates the relationship between the operating temperature ranges of commonly used thermal storage materials and the system's RTE. Currently, thermal storage materials are predominantly used at temperatures below 600 °C. Among them, sensible heat energy storage materials cover a broader temperature range, while latent heat energy storage materials have a relatively narrower and more concentrated applicable range. Therefore, the feasible operating temperature range of TES materials fundamentally constrains the achievable heat storage temperature, thereby indirectly influencing the thermodynamic performance of Carnot battery systems.

The heat storage temperature is closely related to the charging and discharging process of Carnot battery, and the influence of heat storage

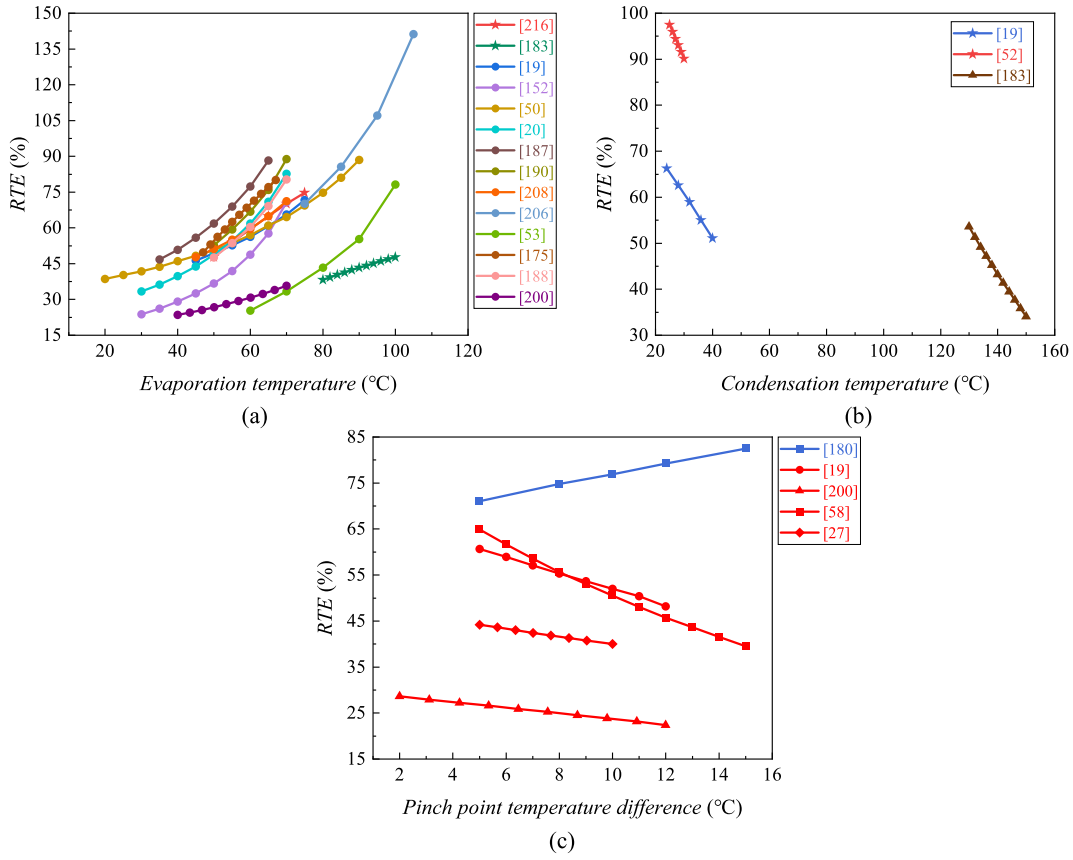


Fig. 13. Effect of heat exchanger parameters on round-trip efficiencies (RTE) of Carnot battery: (a) evaporation temperature, the symbol of "star" represents the discharge process; (b) condensation temperature, the symbol of "star" represents the discharge process; (c) pinch point temperature difference. Data source: (a) [19,20,50,53,152,175,183,187,188,190,200,206,208,216]; (b) [19,52,183]; (c) [19,27,58,180,200].

temperature on RTE exhibits multiple trends across existing studies (see Fig. 14(b) [19,52–54,57,58,64,68,110,183,188,190,200,204,205,208,219]). As shown in the figure, red curves indicate that RTE decreases with increasing heat storage temperature, gray curves show the opposite trend, and blue curves display an initial increase followed by a subsequent decrease [68]. The divergence between the first two trends primarily arises from the opposing effects of storage temperature on the charging and discharging processes: while higher storage temperatures reduce the COP of the HP, they enhance the efficiency of the heat engine. In most ORC systems, the decline in COP is more pronounced, resulting in an overall decrease in RTE as heat storage temperature increases [53,54,146]. Feng et al. (2025) reported an opposite trend under fixed HP condensing temperature, power-generation-side evaporation temperature, and superheat degree [183]. Increasing the heat storage temperature reduced condenser heat rejection, compressor power consumption, and net power output simultaneously. Because the initial condenser heat rejection was substantially larger than compressor power consumption, a comparable absolute reduction resulted in a smaller relative decrease, thereby improving the COP. Since the power-generation-side efficiency remained nearly unaffected, the overall RTE consequently increased. The third trend, characterized by a peak in RTE, occurs because at lower heat storage temperatures, the drop in COP is outweighed by gains in heat engine efficiency, whereas at higher temperatures, the reverse holds true [68]. These divergent trends indicate that the influence of heat storage temperature on RTE is highly dependent on system boundary conditions and the relative sensitivity of charging and discharging efficiencies, rather than following a universally monotonic relationship.

In summary, thermal integration represents a promising pathway to enhance system performance, although its effectiveness depends strongly on heat source quality and system integration strategy. For thermal-integrated systems, increasing both heat source temperature and mass flow rate can enhance thermal input, provided compatibility with component materials and cycle constraints is maintained. Enhancing isentropic efficiency of turbomachinery yields substantial improvements in RTE and power output. However, increasing compressor isentropic efficiency may reduce effective system storage capacity under certain operating conditions due to reduced compressor power input, indicating that efficiency enhancement does not necessarily translate into proportional gains in system-scale performance. Elevating the evaporation temperature improves thermodynamic driving force and cycle efficiency, whereas raising the condensation temperature degrades both RTE and net power output. In both cases, the resulting impact on rated capacity must be explicitly evaluated. To maximize overall performance, the pinch point temperature difference should be minimized within practical design limits, constrained by heat exchanger feasibility, pressure drop, and cost. Heat storage temperature should be optimized rather than maximized, because its influence on RTE depends on the relative sensitivity of charging and discharging efficiencies, while excessively high temperatures may also intensify material degradation, thermal losses, and system cost.

4.3. Sensitivity analysis of LCOS

This section first discusses the influence of system configuration on LCOS. Unlike RTE, which primarily reflects thermodynamic performance, LCOS is jointly determined by both system efficiency and capital expenditure, making it highly sensitive to component performance, operating conditions, and system scale. In Carnot batteries, system costs are predominantly concentrated in key components, including

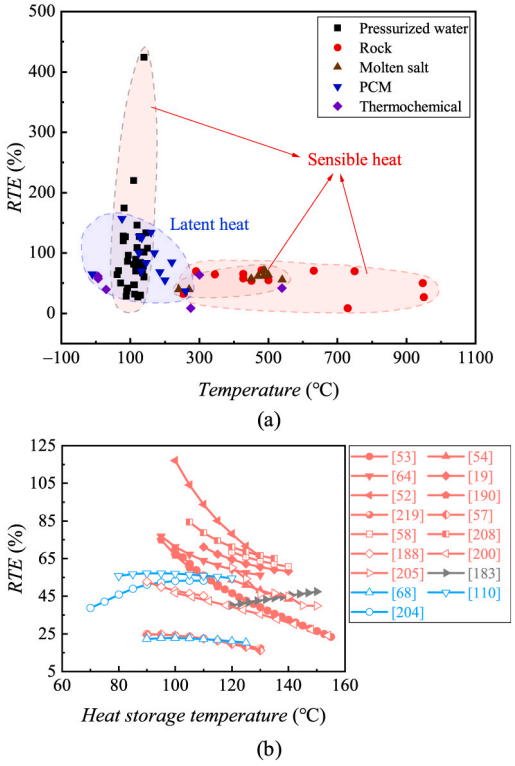


Fig. 14. The temperature range of common thermal storage materials for Carnot battery (a) and effect of the heat storage temperature on round-trip efficiencies (RTE) of Carnot battery when water is used as the heat storage medium (b). Data source: (a) [19,20,25,27,28,33,36,37,45,47–55,58,59,62–64,66,68,74,75,81,104,107,111–114,116,119,121,125,126,129–131,133,138,143,149,151,152,157,159,161,163,167,169,170,175–177,179,180,182,186,193,194,197,204,205,207–210]; (b) [19,52–54,57,58,64,68,110,183,188,190,200,204,205,208,219].

turbomachinery, thermal energy storage tanks, and heat exchangers (the component cost distributions for B-PTES [165] and TI-PTES [54] are shown in Fig. 15). Therefore, improvements in thermodynamic performance do not necessarily translate directly into lower LCOS, highlighting the need for a system-level techno-economic assessment. Accordingly, this section presents a sensitivity analysis to evaluate how key design and operational parameters influence the LCOS, including system parameters, turbomachinery isentropic efficiency, heat exchanger parameters, and heat storage temperature.

4.3.1. *Effect of system configuration on LCOS*

Studies indicate that the LCOS of Carnot battery spans a relatively wide range, approximately 0.065–0.72 $/kWh [194,198], reflecting substantial difference in system configuration, heat source utilization strategy, system scale, and techno-economic assumptions. Representative studies suggest that thermal-integrated configurations generally exhibit stronger economic competitiveness. For example, Brayton-based systems using helium can achieve an LCOS of approximately 0.190 $/kWh under optimized conditions [111], while thermal integration with solar or low-temperature heat sources may further reduce LCOS to around 0.168 $/kWh [218]. Geothermal-assisted systems have reported even lower values, reaching 0.065 $/kWh after optimization [198], demonstrating strong economic competitiveness. Fig. 16 [19,20,29,53,54,56–58,63–68,75,92,93,110,111,115,116,119,132,150–152,164,166,171,173,175,177,180,182,183,187,188,190,192–194,196,198,199,201,207,209,214,216,218–221] shows the LCOS distribution of different configurations of Carnot battery.

Among these studies, Yin et al. utilized geothermal energy during both charging and discharging processes, optimized the compressor outlet pressure, increased geothermal temperature, and matched different optimal configurations to different geothermal temperature levels. As a result, the LCOS of the Carnot battery was reduced to as low as 0.065 $/kWh [198]. Hu et al. also confirmed that thermal integration using geothermal energy can achieve a more attractive LCOS [20], although its application is constrained by geographical conditions. Given the limited availability of geothermal resources, thermal-integrated systems utilizing continuous and cost-free waste heat are expected to achieve even lower LCOS.

Thus, TI-PTES generally exhibits greater potential for achieving lower LCOS owing to its ability to utilize external heat sources and improve overall energy utilization efficiency. This economic advantage highlights TI-PTES as a promising development pathway for Carnot battery. Nevertheless, achieving low LCOS in practical deployment still requires efficient heat source integration, suitable site conditions, and effective coordination between system complexity and capital investment.

4.3.2. *Effect of system parameters on LCOS*

For thermal-integrated systems, heat source conditions are critical because they govern both system utilization and achievable power output, thereby directly affecting LCOS. Installed capacity strongly influences capital expenditure, whereas operation duration determines annual utilization and cost amortization. Consequently, LCOS is governed not only by thermodynamic performance but also by the balance between system scale, utilization intensity, and investment cost.

Thermal integration represents one of the most promising pathways for improving the economic viability of Carnot battery, particularly when stable and suitable external heat sources are available. The characteristics of the heat source, specifically temperature and mass flow rate, directly influence the system's economic performance in applications such as industrial waste heat recovery. As shown in Fig. 17(a) [68,132,188,198], LCOS generally decreases with increasing heat source temperature. Although higher heat source temperatures may slightly reduce annual power generation, the reduction in total

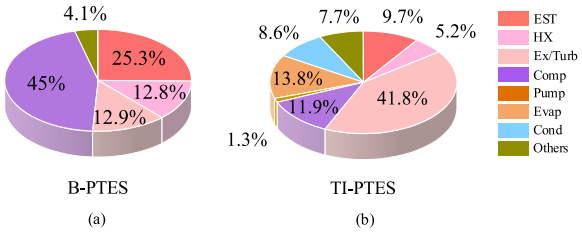


Fig. 15. Cost distribution in Carnot battery of (a) B-PIES [165] and (b) TI-PTES [54].

investment and operating costs is more pronounced, thereby lowering LCOS [68]. Moreover, excessively high heat source temperatures may introduce additional engineering challenges, including material durability requirements and increased system complexity, implying that economic optimization should balance thermodynamic gains against implementation cost. Similarly, an increase in heat source mass flow rate contributes to a lower LCOS (see Fig. 17(b) [180,188]), as the system operates at a higher capacity utilization level, and the resulting gain in net power generation outweighs the associated rise in capital expenditure [180]. However, when the mass flow rate exceeds a certain threshold, the rate of LCOS reduction gradually diminishes. This is because, at very large scales, the costs of key components, such as high-power turbomachinery and large-scale thermal storage tanks, increase nonlinearly due to challenges in design, material selection, and manufacturing complexity. Combined with higher expenses for fabrication, transportation, and maintenance, this results in a "diseconomy of scale" effect. This result suggests that scaling up thermal-integrated systems does not guarantee proportional economic benefits, and the economically optimal capacity should be determined through system-specific techno-economic optimization.

Installed capacity is a key factor influencing the LCOS. As shown in Fig. 18 [111], increasing installed capacity generally leads to economies of scale, thereby reducing LCOS [111,173,222]. This occurs because the growth rate of total investment cost, particularly for power-related components, is typically lower than that of total discharged energy, resulting in a lower fixed cost allocation per unit of electricity. However, the economic benefit of capacity expansion is not unlimited. At very large scales, nonlinear increases in equipment cost, engineering complexity, and infrastructure requirements may weaken the cost reduction effect, highlighting the importance of balancing economies of scale against rising system complexity and implementation costs.

The system operational duration, which includes the charging duration and annual utilization hours, directly governs asset utilization and capital cost amortization. For a given charge and discharge duration, annual utilization hours are closely associated with the annual cycling frequency. As shown in Fig. 19(a) [173,180,188,222], the LCOS decreases with increasing charging duration. Although a longer charging duration necessitates higher investment in thermal storage systems, the associated increase in total discharged electrical energy is more substantial, leading to a net reduction in LCOS. Meanwhile, annual utilization hours serve as a key indicator of asset utilization. Increasing this parameter allows the same capital investment to generate more electricity over time, thereby significantly reducing LCOS [20,65,115,216] (see Fig. 19(b) [20,65,216]). Therefore, improving the capacity factor through higher annual utilization and rationally extending charging duration represents an effective pathway to reducing LCOS. However, the economic benefit is ultimately constrained by electricity market conditions, heat source availability, and operational flexibility requirements, implying that excessively long charging duration or unrealistic utilization assumptions may overestimate practical economic performance.

4.3.3. *Effect of turbomachinery efficiency on LCOS*

The isentropic efficiency of turbomachinery exerts a nearly linear influence on LCOS (see Fig. 20 [20,216]). Improved isentropic efficiency directly enhances RTE, thereby increasing electricity output for a given energy input or reducing equipment requirements for the same output target. Fig. 20 further reveals that LCOS is more sensitive to turbine efficiency than to compressor efficiency because the turbine discharge process has a significant impact on the total investment cost [216]. Therefore, investing in high-performance turbomachinery, particularly turbines, is generally favorable from a lifecycle LCOS perspective. However, the economic benefit depends on whether efficiency gains outweigh the additional capital and maintenance costs associated with advanced turbomachinery technologies.

4.3.4. *Effect of heat exchanger parameters on LCOS*

The heat exchanger parameters directly influence the exergy losses and required heat transfer area of Carnot battery. The selection of evaporation temperature requires balancing its competing effects on thermodynamic performance, component sizing, and system economics. As illustrated in Fig. 21(a) [19,20,53,152,175,183,188,190,200,216], the relationship between evaporation temperature and LCOS exhibits two distinct trends. In most studies, LCOS initially decreases and subsequently increases with rising evaporation temperature. During the charging process, a higher evaporation temperature reduces compressor power consumption and overall system power, leading to a decline in total investment cost (C_{inv}). However, because system power decreases more rapidly than total investment cost, the unit investment cost (C_{inv}/W_{comp}) increases, resulting in excessive system downsizing and weakened economies of scale. Consequently, the dominant economic driver gradually shifts from total investment cost to unit investment cost, giving rise to an optimal evaporation temperature that minimizes LCOS [152]. During the discharging process, increasing evaporation temperature generally enhances power output and reduces LCOS. However, further increases may require a larger thermal energy storage unit and substantially higher investment cost, which can ultimately reverse the declining trend in LCOS [216]. In some studies [53,175,183], specific heat source conditions keep the system within the declining phase of LCOS, yielding a continuously decreasing trend. These divergent results demonstrate that evaporation temperature must be optimized according to actual operating conditions, as no universal optimal value exists.

Increasing the condensation temperature generally leads to a progressive decline in RTE and a corresponding rise in LCOS, as illustrated in Fig. 13(b) and Fig. 21(b) [19,183], respectively. An increase in condensation temperature elevates both investment and annual operating costs and ultimately increases LCOS. Even when power output remains stable or increases marginally under certain operating conditions, the resulting economic benefit is generally insufficient to offset the associated cost escalation [19,183].

As shown in Fig. 21(c) [19,58,180,200], reducing the pinch point temperature difference can minimize exergy destruction and enhance thermodynamic efficiency. However, this necessitates a larger heat

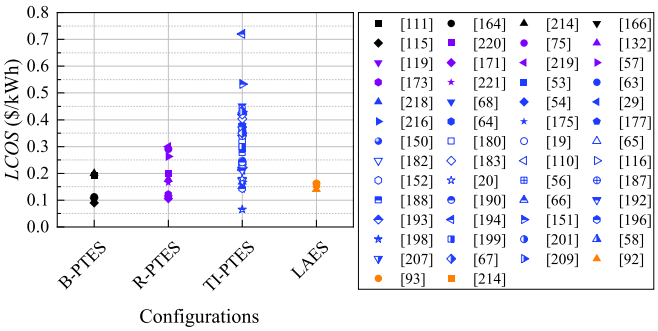


Fig. 16. Effect of configurations of Carnot battery on levelized cost of storage (LCOS) (TI-PTES includes TI-BPTES and TI-RPTES). Data source: [19,20,29,53,54,56–58,63–68,75,92,93,110,111,115,116,119,132,150–152,164,166,171,173,175,177,180,182,183,187,188,190,192–194,196,198,199,201,207,209,214,216,218–221].

transfer area, thereby increasing investment costs. Conversely, increasing the pinch point temperature difference reduces investment cost but degrades system efficiency, leading to a higher LCOS [19,54]. An optimal pinch point temperature difference exists: increasing pinch point temperature difference from its lower bound primarily reduces heat exchanger investment cost, whereas further increases beyond the upper bound predominantly degrade RTE [200]. Specifically, RTE is most sensitive to the pinch point temperature difference of HP. This is because the temperature difference directly affects the COP of the HP, and changes in COP typically have a greater influence on RTE than variations in ORC efficiency. Meanwhile, LCOS is most sensitive to the pinch point temperature difference of ORC, since the discharge process has a strong influence on the total investment cost [20,216]. This difference highlights that optimizing heat exchanger parameters based solely on thermodynamic performance may not necessarily lead to the lowest LCOS, underscoring the need for system-level co-optimization between charging and discharging subsystems.

4.3.5. *Effect of heat storage temperature on LCOS*

Heat storage temperature is a pivotal parameter affecting both the thermodynamic performance and economic viability of the system. As illustrated in Fig. 22 [19,53,54,56–58,64,68,110,187,188,190,200,209,219], studies show that LCOS typically follows a nonlinear trend, initially decreasing and then increasing with rising heat storage temperature [200]. In the low-temperature range, increasing the storage temperature significantly improves heat engine efficiency and power output, which dominates the reduction in LCOS despite a slight decline in RTE due to reduced COP [54]. At higher temperatures, stricter equipment requirements lead to increased investment costs [200]. The divergence between the red and gray curves in the figure primarily arises from differences in their operating conditions [53,187,209], corresponding to distinct optimal temperature ranges for minimizing LCOS. This indicates that no universally optimal heat storage temperature exists. Therefore, the optimal thermal storage temperature should be determined according to specific operating conditions, with careful consideration given to the trade-off between system efficiency and cost.

The economic performance of Carnot battery constitutes a multivariable coupled optimization problem, in which maximizing thermodynamic performance does not necessarily minimize LCOS. To reduce LCOS, refined optimization of heat transfer parameters and heat storage temperature should be conducted during the design phase, ensuring proper matching with available heat sources and system operating conditions. During operation, dispatch strategies should be optimized to maximize annual utilization hours and capacity factor, thereby improving asset utilization and economic returns. Furthermore, expanding system scale and investing in high-efficiency core power equipment represent important pathways to lowering unit costs, although the economic benefits may gradually diminish at very large scales due to increasing system complexity and infrastructure requirements. Future technological development and engineering practice should therefore prioritize system-level synergistic optimization of thermodynamic performance, component cost, and operational flexibility to accelerate the commercialization of Carnot battery systems.

4.4. *Summary of system performance and economy analysis*

This section details the key indicators used to evaluate the thermodynamic and economic performance of Carnot batteries, namely RTE and LCOS. TI-PTES demonstrates strong thermodynamic and economic potential because external heat utilization effectively enhances system performance, making it a promising configuration. Higher heat source temperature and flow rate generally contribute to lower LCOS, while improving turbine isentropic efficiency deserves greater priority than compressor efficiency. System performance depends more on thermal matching and parameter coordination than on universally optimal operating conditions: minimizing the pinch point temperature difference is generally beneficial, whereas evaporation and condensation temperatures require case-specific optimization due to trade-offs among efficiency, net power output, and rated capacity. Apparent inconsistencies in sensitivity analysis mainly arise from differences in system boundary assumptions.

The development of Carnot battery thermodynamic and economic performance has shown a clear divergence between rapid theoretical advancement and limited engineering verification. Early studies established the analytical foundation for PTES by providing systematic thermodynamic frameworks and practical component loss estimation methods, enabling subsequent optimization studies to move beyond conceptual feasibility toward quantitative performance comparison [61,62]. Building on this basis, TI-PTES emerged as a major technological pathway after Frate et al. demonstrated that introducing external heat above ambient temperature could increase electricity output without additional electrical input [146]. This fundamentally expanded the optimization direction of Carnot batteries by introducing the utilization of external heat sources and thermal matching to improve thermodynamic and economic performance. Consequently, theoretical studies reported increasingly attractive performance limits, including RTE exceeding 200% through thermal-integrated dual-pressure configurations [197] and LCOS values as low as 0.065 $/kWh under geothermal assistance [198].

However, the rapid growth of theoretical performance indicators has not been matched by experimental progress. More importantly, the discrepancy is not merely quantitative but structural. Existing experiments remain fragmented in scope: system-level works verified the feasibility of TI-PTES [210], reversible HP–ORC studies exposed the

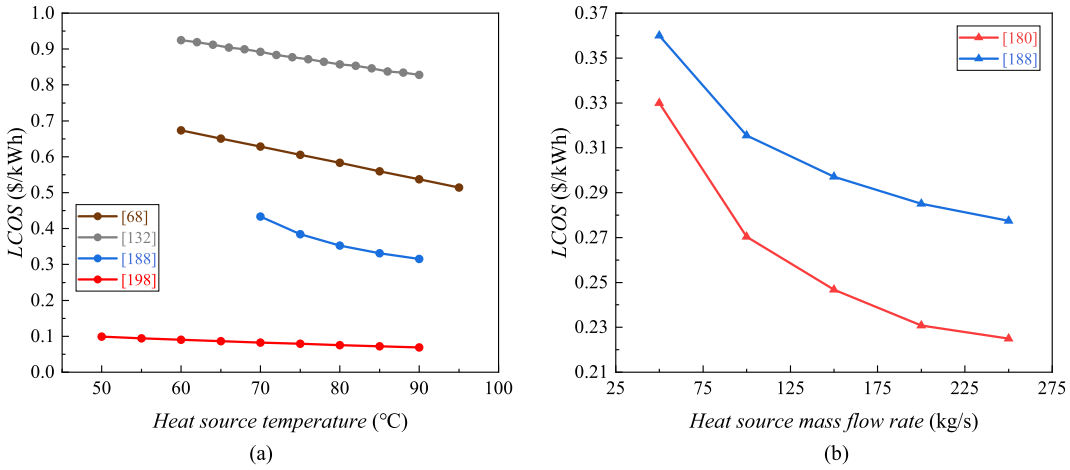


Fig. 17. Effect of heat source temperature (a) and heat source mass flow rate (b) on the levelized cost of storage (LCOS) of Carnot battery under thermal integration conditions. Data source: (a) [68,132,188,198]; (b) [180,188].

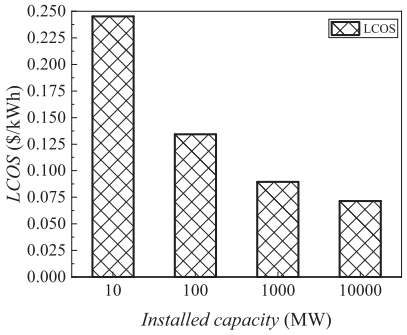


Fig. 18. Effect of installed capacity on the levelized cost of storage (LCOS) of Carnot battery. Data source: [111].

practical efficiency penalties of shared machinery [107], while TES unit experiments clarified the performance enhancement mechanisms and irreversibility sources of cascaded latent heat storage in B-PTES [167]. Yet no study has simultaneously demonstrated highly efficient reversible compression/expansion, low-loss thermal storage, and effective thermal integration within a unified Carnot battery system. As a result, the remarkable theoretical gains in RTE and LCOS still rely heavily on idealized assumptions, including favorable external heat sources availability, optimistic component efficiencies, and highly coordinated thermal management strategies. Therefore, the key challenge in Carnot battery development is no longer proving theoretical feasibility, but establishing experimentally validated system integration capable of translating thermodynamic potential into reproducible engineering performance.

5. Current status of commercial application

As a key technology for long-duration energy storage, Carnot battery has demonstrated significant advantages in both thermodynamic efficiency and economic feasibility. Fueled by the growing global demand for reliable energy storage solutions during the energy transition, the technology has rapidly progressed from laboratory research to engineering demonstration and early commercial deployment, with representative projects summarized in Table 4 [223–241]. Nevertheless, despite the successful grid connection and operation of several demonstration projects, large-scale commercialization remains constrained by challenges associated with system integration, off-design operation, thermal management, and cost reduction. This section describes global demonstration initiatives and commercial advancements of Carnot battery, as well as the main challenges for its industrialization.

5.1. Global major demonstration projects and technology routes

The commercialization progress of Carnot battery exhibits distinct characteristics that are closely tied to their respective technical pathways. LAES has achieved significant advancement in grid-scale large-scale energy storage, driven by its high energy density. The 50 MW/300 MWh project developed by Highview Power in Carrington, UK, and the 100 MW/1 GWh commercial-scale project pursued by Everllence in Germany mark the entry of this technology into the early stage of commercialization [225,233], demonstrating its viability for long-duration energy storage and grid support services.

In the domain of industrial energy services, HP-ORC systems have demonstrated unique application potential. A demonstration project at Xisai Science Valley in Huzhou, Zhejiang, successfully delivers 380 °C industrial steam using an 8 MW ultra-high-temperature HP, validating the technical pathway for converting electrical energy into high-grade thermal energy [230,231]. Meanwhile, the modular TWEST system developed by E2S-power integrates electrical-to-thermal conversion with thermal storage units, lowering the barrier to low-carbon industrial transition through its innovative “steam as a service” business model [234].

Carnot battery also plays a critical role in the transformation of conventional energy infrastructure. The ETES pilot project implemented by Siemens Gamesa in Hamburg employs resistive heating combined with volcanic rock-based thermal storage to achieve 130 MWh of

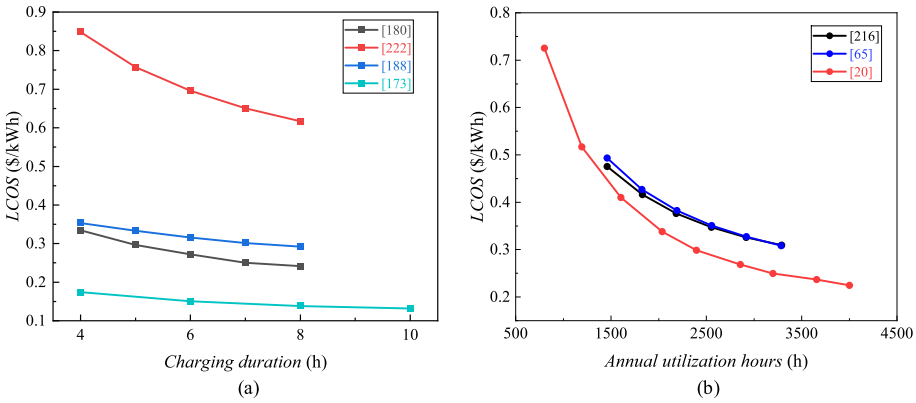


Fig. 19. Effect of the charging duration (a) and annual utilization hours (b) on the levelized cost of storage (LCOS) of Carnot battery. Data source: (a) [173,180,188,222]; (b) [20,65,216].

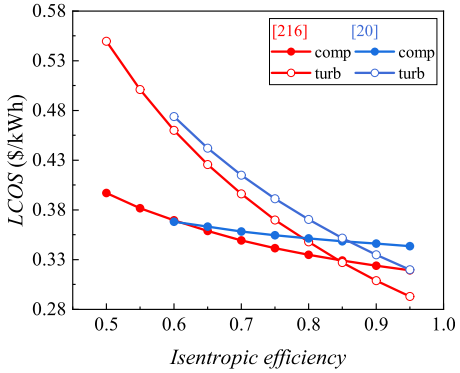


Fig. 20. Effect of isentropic efficiency of turbomachinery on the levelized cost of storage (LCOS) of Carnot battery (comp: compressor; turb: turbine). Data source: [20,216].

electrical-to-thermal conversion and storage, offering a viable technical blueprint for repurposing retired coal-fired power plants [227,228]. Similarly, Pintail Power's proposed liquid salt combined cycle and liquid air combined cycle technologies enable the transformation of legacy power assets into flexible energy storage resources by deeply integrating hot and cold storage systems into existing plant configurations [240,241], thereby significantly reducing marginal investment costs.

From the standpoint of technology maturity, R-PTES, B-PTES and LAES have advanced to the early commercialization phase [228,232]. The GridScale demonstration project by Stiesdal in Denmark utilizes packed-bed thermal storage with gravel, representing a strategic effort to improve the cost-effectiveness of B-PTES [229]. The commissioning of the Chuno project in China has provided a solution for stabilizing renewable energy generation and improving project economics in the pursuit of decarbonization pathways. The project is capable of supplying heat, cooling, and electricity [232].

Among the currently verified Carnot battery projects worldwide, the RTE of R-PTES exceeds 75% and the LCOS reaches 0.1 $/kWh [223,224], that of LAES can reached 70% [225], while that of B-PTES ranges from 55% to 65% [229,232], yet remains significantly below theoretical predictions. This performance gap highlights the persistent influence of practical engineering constraints, including thermal losses, subsystem coordination challenges, auxiliary energy consumption, and off-design operation. From a grid perspective, only 0.55–0.75 kWh of electricity is recoverable per kWh ultimately consumed. Therefore, improving real-world operational performance while maintaining favorable thermodynamic and economic performance remains essential for the large-scale deployment of Carnot battery systems.

In summary, Carnot battery, leveraging its technological diversity, offers adaptable solutions for applications in power systems, industrial processes, and the retrofitting of traditional energy facilities. Rather than converging toward a single universal solution, future commercialization of Carnot battery is likely to involve differentiated technical pathways tailored to specific application scenarios. Among these, thermal-integrated systems are expected to represent a particularly promising development direction owing to their superior potential for enhancing thermodynamic and economic performance through effective utilization of external heat sources. Nevertheless, widespread deployment continues to face substantial technical, economic, and regulatory challenges.

5.2. Main challenges

Carnot battery can achieve energy storage capacity at the GWh scale [225,241], and larger capacities enable stronger capabilities to mitigate renewable generation fluctuations and improve power system flexibility [242]. However, large-scale deployment faces numerous challenges that currently hinder their commercialization.

The commercialization of Carnot battery faces several key challenges, including high total investment costs, complex system integration, and unclear transient characteristics. Among these, the capital expenditures associated with critical components such as compressors and expanders represent the primary financial barrier. The technology requires interdisciplinary integration, and the high complexity involved in its design, system integration, and operation and maintenance has, to some extent, impeded large-scale deployment. Although significant progress has been made in the theoretical research on Carnot batteries, actual operational data remain scarce, and empirical assessments of efficiency and economic viability are still limited [243].

More importantly, the foremost technical bottleneck for realizing high-efficiency and grid-compatible Carnot batteries lies in the inability to accurately predict and control transient behaviors under off-design

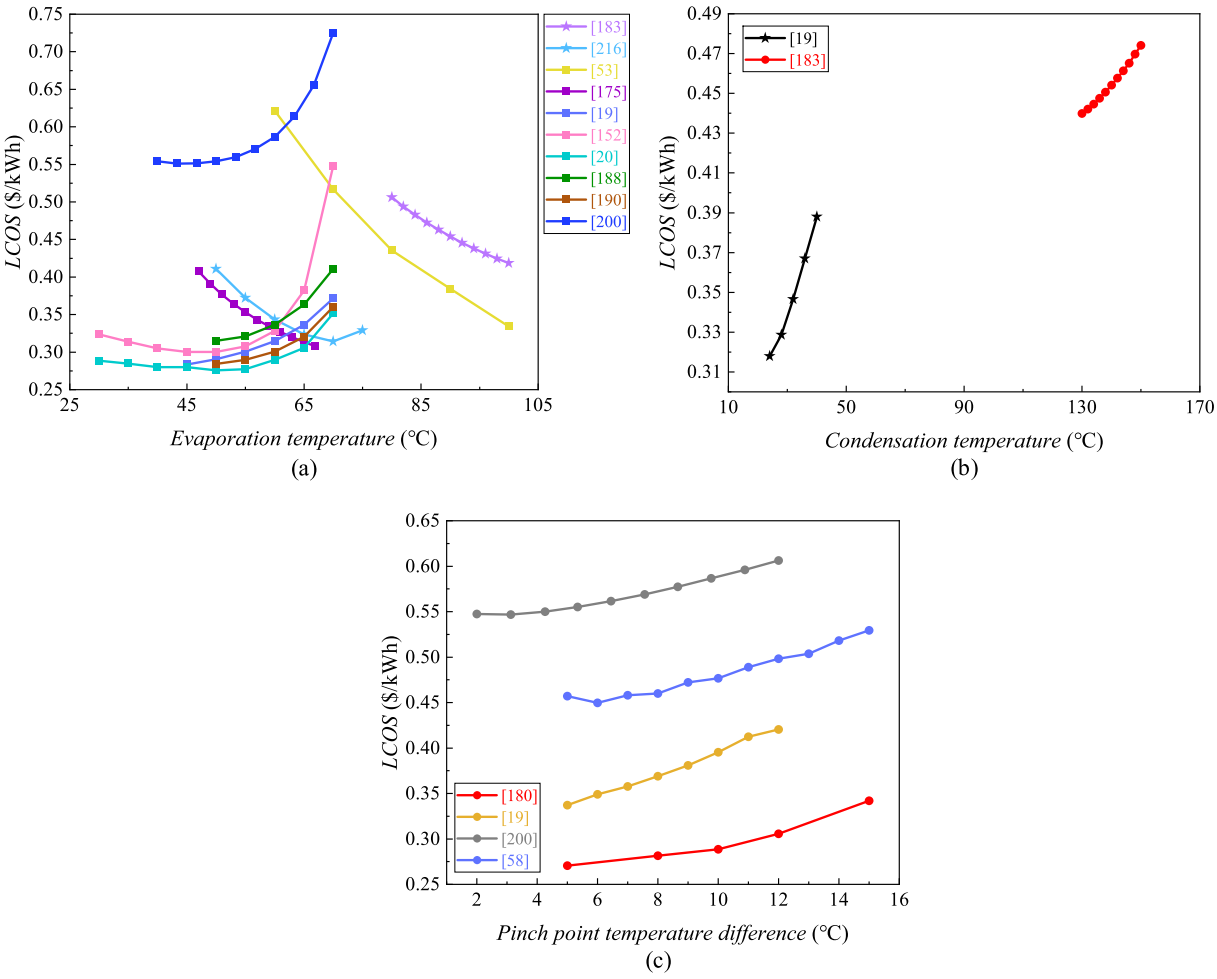


Fig. 21. Effect of heat exchanger parameters on the levelized cost of storage (LCOS) of Carnot battery: (a) evaporation temperature, the symbol of "star" represents the discharge process; (b) condensation temperature, the symbol of "star" represents the discharge process; (c) pinch point temperature difference. Data source: (a) [19,20,53,152,175,183,188,190,200,216]; (b) [19,183]; (c) [19,58,180,200].

operating conditions. Existing steady-state models are inadequate for this purpose, and a well-developed dynamic control framework is still missing [244]. This mismatch between nominal-condition modeling and real operational requirements constitutes a fundamental barrier to practical deployment.

A research team from Leibniz University Hannover explicitly identified "off-design operation" as the analytical core for this issue [245]. Pecchini et al. showed through off-design simulations that using simplified design-point models to evaluate partial-load performance leads to a calculation error in discharge depth of 7% to 23% [128]. This error indicates that ignoring off-design characteristics causes significant misjudgment of system economics and efficiency.

In addition, the efficiency of key components (e.g., compressors and expanders) can deviate substantially under partial-load conditions, making nominal performance maps unreliable [246]. This further complicates dynamic system regulation and underscores the need for accurate off-design models integrated with dedicated control strategies. Some studies have attempted to build dynamic models for off-design conditions and investigated corresponding control strategies [157,245,247]. However, even the most promising inventory control strategy covers only 61.4% of the theoretical nominal operating range and demonstrates modest performance. The PID controller recently designed by Pecchini et al. achieved a power setting time of about 1.2–3.3 s and a shaft speed fluctuation within 1.4% on a 10 MW Brayton cycle-based Carnot battery for a power step from 60% to 100% [248]. Some studies have achieved rapid tracking and low-disturbance energy transfer in multi-energy supply systems through temperature matching control [249]. In addition, composite control strategies (feedforward + PID) have improved response speed by more than 55% compared with conventional PID control, significantly enhancing resistance to heat source disturbances [250]. However, these methods remain limited in prediction and constraint-handling capabilities when dealing with wide-ranging operating conditions, strong nonlinearities, and multi-objective economic optimization.

Therefore, the inability to predict and control off-design transient behavior deserves priority attention in Carnot battery development. Overcoming this bottleneck is essential not only for stable system operation, but also for translating theoretical performance advantages into practically achievable high-RTE and low-LCOS Carnot batteries.

To address the limitations of dynamic models under off-design conditions, this paper recommends introducing a 1D/3D coupled multiscale modeling approach, which may offer potential breakthroughs [251,252]. In studies of dynamic operation, purely 1D models are computationally efficient but show insufficient predictive accuracy under off-design conditions [128], whereas purely 3D models provide high accuracy at the expense of substantial computational cost, making long-term dynamic analysis of the entire system impractical. The development of a 1D/3D coupled multiscale framework could balance

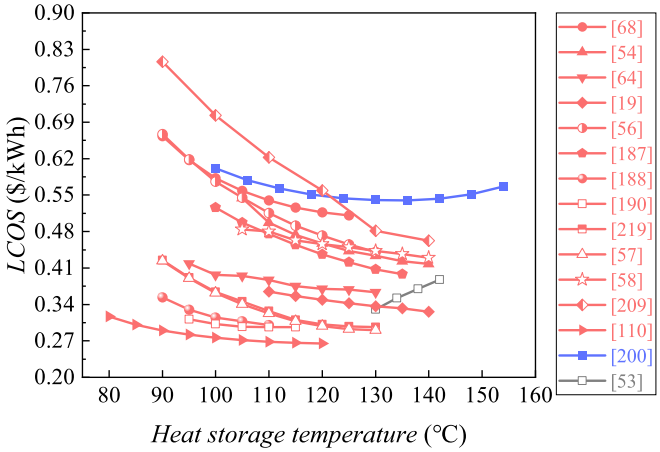


Fig. 22. Effect of the heat storage temperature on the levelized cost of storage (LCOS) of Carnot battery when water is used as the heat storage medium. Data source: [19,53,54,56–58,64,68,110,187,188,190,200,209,219].

global response speed and local predictive accuracy at a manageable computational cost. Taking the B-PTES configuration as an example, 3D high-fidelity simulations could be applied to key components, such as storage tanks and turbomachinery, which exhibit large thermal inertia and high sensitivity to efficiency variations under off-design conditions, respectively. While 1D simplified models could be adopted for the remaining subsystems, including pipelines and heat exchangers.

To address control strategy challenges, nonlinear model predictive control (NMPC) may offer a promising direction. Li et al. [253] demonstrated that NMPC can reduce supply-demand deviations by approximately 25%–33% while lowering operating costs by 16%. Naik et al. [254] further proposed a multi-stage economic NMPC approach that incorporates extreme scenarios and Lyapunov constraints, enabling more stable satisfaction of economic and safety requirements under uncertain disturbances. Therefore, an NMPC framework integrating economic optimization with robust predictive capability is expected to significantly enhance the transient control performance of Carnot batteries under intense load fluctuations.

5.3. Summary of commercial progress

Existing demonstration projects indicate that the application scope of Carnot batteries is expanding from electricity storage and power generation to broader functions within energy systems, including grid fluctuation balancing, industrial heat supply, and the reutilization of conventional energy infrastructure [225,227,230,232]. The diversification of technological pathways reflects increasingly diverse application demands. However, the gap between theoretical and practical performance suggests that current research still relies heavily on steady-state models and idealized assumptions, while accurate prediction and control under transient and off-design conditions remain insufficient. Future progress therefore depends on developing high-fidelity dynamic models, where 1D/3D coupled multiscale modeling and NMPC may provide promising pathways for improving operational flexibility and dynamic performance [252,253].

6. Conclusions and prospects

This paper reviews the development of Carnot battery from the perspectives of system configuration, key component and commercialization progress. The influence on techno-economic indexes is mainly discussed, including round-trip efficiency (RTE) of Carnot battery and levelized cost of storage (LCOS).

6.1. Conclusions

In the development process of Carnot battery, various configurations are proposed successively, including Brayton cycle-based pumped thermal energy storage (B-PTES), Rankine cycle-based pumped thermal energy storage (R-PTES), thermal-integrated pumped thermal energy storage (TI-PTES), etc. Based on the comprehensive review of Carnot battery technologies from the perspectives of system configuration, key components, and commercialization progress, the main conclusions can be summarized as follows:

- At the system level, TI-PTES is identified as the potential configuration in future. According to recent theoretical investigations, its RTE can rise up to 220% when using optimized R1233zd(E)/cyclopentane mixtures for charging and discharging separately, combined with a dual-pressure discharge cycle and a longer discharging duration. Its LCOS can be reduced to 0.065 $/kWh under the conditions of a geothermal temperature of 90 °C and a compressor outlet pressure of 5.5 MPa when R1336mzz(Z) is used as the working fluid.
- Among Carnot battery configurations, R-PTES began to appear in the engineering application, the RTE and LCOS are about 75% and 0.1 $/kWh, respectively.
- At the component level, the operating parameters of heat exchanger and turbomachinery behave important influence on the RTE and LCOS. Specifically, decreasing the pinch point temperature difference of heat exchanger and increasing isentropic efficiencies of turbomachinery are the effective pathways to rise RTE and reduce LCOS. There exists an optimal evaporation temperature during discharge process to obtain the minimum LCOS.

6.2. Prospects

Although significant progress has been achieved in recent years, several technical, economic, and commercialization challenges still remain. To further improve system performance and facilitate large-scale deployment, future research directions are summarized as follows:

- Among the present investigations of Carnot battery, the experimental data is limited and the engineering application is rare. Thus, it is important task to obtain operating data in future. What is more, off-design transient behavior needs to be especially concerned, ensuring high RTE in all operating states and low LCOS with benefits from flexible operation.
- To address the limitations of dynamic models under off-design conditions, future research could develop 1D/3D coupled multiscale

Table 4
Typical Carnot battery demonstration projects.

Projects	Country	Year	TES material	System configuration	Power /Capacity	Application status	RTE (%)	Project-related information	Ref.
Energy Dome's CO2 Battery	Italy	2022	Liquid CO_2	R-PTES	MW level/—	Grid-connected operation	>75	Using CO_2 as the working fluid, and the service life is over 30 years, the LCOS is as low as 0.1 $/kWh.	[223,224]
Everllence LAES	Germany	2025	Liquid air / packed bed / molten salt	LAES	50–250 MW/3.2 GWh	Commercial promotion	55–70	The service life is over 35 years, and zero performance degradation.	[225]
1414° SiBox	Australia	2024	SiBricks	B-PTES	—/MWh-GWh	Complete the demonstration	–	Supplies clean heat reaching 1000 °C, zero major overhaul, flexible layout, high energy density, safe and efficient.	[226]
Siemens Gamesa ETES	Germany	2019	Volcanic rock	R-PTES	—/130 MWh	Trial run	25 ~ >40	Electric heating for charging, with a heat storage temperature reaching 750 °C, the pilot power plant's heat storage can last for a week.	[227,228]
GridScale System	Denmark	2023	Gravel	B-PTES	2 MW/—	Demonstration run	55–60	It can cope with the full-cycle fluctuations ranging from several hours of photovoltaic to several days of wind energy, with a COP of approximately 250%.	[229]
The ultra-high-temperature PTHS	China	2025	Molten salt	R-PTES	8 MW/—	Demonstration run	–	The largest ultra-high temperature pumped thermal heat storage in the world, COP reaching 130%–200%, with a steam output of 11.5 t/h, a steam temperature of 380 °C, and a pressure of 1 MPa.	[230,231]
Chuno	China	2025	Molten salt	B-PTES	1 MW/4 MWh	Demonstration run	> 65	World-first 560°C Carnot battery, uses air as the working fluid, energy density of 80–120 kWh/m^3, the heat storage temperature is higher than 560°C, while the cold storage temperature is as low as −60°C.	[232]
Carrington LAES	Britain	2025	Liquid air	LAES	50 MW/ 300 MWh	Under construction	–	The largest commercial-scale LAES in the world.	[233]
E2S-power TWEST	Switzerland	–	Graphite-aluminium alloy	R-PTES	MW level/—	Commercial verification	25–40	Modular design integrates electric boilers and heat storage to provide decarbonized steam, high flexibility, almost no performance degradation, no deep discharge issues, and a long service life.	[228,234,235]
Echogen PTES	USA	–	Water, concrete	R-PTES	50–200 MW/—	Commercial verification	~60	Using supercritical CO_2 as the working fluid, it features high flexibility and reliability, material safety, long service life and small floor space.	[236]
TEXEL Energy Storage	Sweden	–	Metal hydrides / metal carbonates	SC-PTES	30 kW/ 15–720 kWh	Under development in technology	40	Provides 6-h to seasonal energy storage to address the intermittency of renewable energy, with high recyclability, long service life, low performance degradation.	[228,237]
WindTP system	Britain	–	Gravel-packed bed	B-PTES	3–20 MW/—	Under development in technology	85	Wind turbine integrated thermal storage system, supplies 25–100 h of rated turbine output, with low marginal cost, high performance, and flexible siting.	[238]
NewAtlas thermal battery	Australia	2019	Silicon	SC-PTES	—/1.2 MWh	Under development in technology	–	Modular design, energy density six times that of lithium-ion, convenient for scale expansion, and no capacity degradation.	[239]
PintailPower LSCC	USA	–	Molten salt	R-PTES / B-PTES	MW level/—	Conceptual design	82–96 (+fuel)	Responds rapidly to the fluctuations of renewable energy, is flexible and efficient, and typically has a heat loss of less than 1°C per day.	[228,240]
PintailPower LACC	USA	–	Liquid air	LAES	—/10+ GWh	Conceptual design	118 (+fuel)	Ultra-large-scale LAES, high energy density, plentiful and non-toxic air.	[228,241]

modeling approaches to balance global response speed and local predictive accuracy at a manageable computational cost.

- To address control strategy challenges, nonlinear model predictive control (NMPC), integrating economic optimization with robust predictive capability, is expected to significantly enhance the transient control performance of Carnot battery under off-design operating conditions.
- The conventional, first-law definition of RTE does not account for the quality of external heat sources. In contrast, the second-law RTE evaluates system performance from an exergy-based perspective, yielding results that are more rigorous and thermodynamically sound. Therefore, this second-law metric warrants further investigation and application.

CRediT authorship contribution statement

Anbu Chen: Writing – original draft, Visualization, Formal analysis. **Huan Liu:** Visualization, Investigation, Data curation. **Qiuru Dong:** Validation, Methodology, Data curation. **Jinliang Xu:** Writing – review & editing, Supervision, Funding acquisition. **Jian Xie:** Writing – review & editing, Project administration, Conceptualization.

Declaration of competing interest

The authors declare that they have no known competing financial interests or personal relationships that could have appeared to influence the work reported in this paper.

Acknowledgments

The authors acknowledge the support from National Natural Science Foundation of China (No. 52130608) and the Fundamental Research Funds for the Central Universities (No. 2026TX006 and 2020DF002).

Data availability

Data will be made available on request.

References

[1] T. Appenzeller, Good morning, sunshine, Science 390 (6779) (Dec. 2025) 1208–1209, https://doi.org/10.1126/science.aee8000.
[2] S. Impram, S. Varbak Nese, B. Oral, Challenges of renewable energy penetration on power system flexibility: a survey, Energy Strat. Rev. 31 (Sep. 2020) 100539, https://doi.org/10.1016/j.esr.2020.100539.
[3] F. Wang, Y. Xue, A review of the development of the energy storage industry in China: challenges and opportunities, Energies 18 (6) (Mar. 2025) 1512, https://doi.org/10.3390/en18061512.
[4] Efstathios E. Michaelides, Electrochemical storage–batteries, in: Energy Storage, 1st edition, CRC Press, 2025, p. 44, https://doi.org/10.1201/9781003380085.
[5] Karlsruhe Institute of Technology, Scenario 2050: Lithium and Cobalt might not suffice, Accessed: Feb. 24, 2026. [Online]. Available: https://www.kit.edu/kit/english/pi_2018_027_scenario-2050-lithium-and-cobalt-might-not-suffice.php, March 14, 2018.
[6] M. Mahnoor, R. Chandio, A. Inam, I.U. Ahad, Critical and strategic raw materials for energy storage devices, Batteries 11 (4) (Apr. 2025) 163, https://doi.org/10.3390/batteries11040163.
[7] T. Yang, et al., The role and substitution of cobalt in the cobalt-lean/free nickel-based layered transition metal oxides for lithium ion batteries, Batteries Supercaps 7 (12) (Dec. 2024) e202400437, https://doi.org/10.1002/batt.202400437.
[8] W.-J. Cho, Y.J. Huh, S. Choi, U. Kulkarni, K.P. Shejale, G.-R. Yi, Innovations in non-flammable and flame-retardant electrolytes for safer lithium-ion batteries, Chem. Commun. 61 (65) (2025) 12056–12068, https://doi.org/10.1039/D5CC01203A.
[9] J. Xie, Y. Lu, Designing nonflammable liquid electrolytes for safe Li-ion batteries, Adv. Mater. 37 (2) (Jan. 2025) 2312451, https://doi.org/10.1002/adma.202312451.
[10] Y. Zeng, T. Zhou, T. Wang, M. Zhang, S. Zhang, H. Yang, Long-duration energy storage: a critical enabler for renewable integration and decarbonization, Energies 18 (3) (Jan. 2025) 466, https://doi.org/10.3390/en18030466.
[11] Claire Turvill, Nickel-Iron 'Battolyser' for Long-term Renewable Energy Storage and Clean Fuel Production, Accessed: Feb. 24, 2026. [Online]. Available: https://eepower.com/news/nickel-iron-battolyser-for-long-term-renewable-energy-storage-and-clean-fuel-production/?trk=article-ssr-frontend-pulse_little-text-block#, Sep 15, 2022.
[12] Z. Dong, Y. Tao, S. Lai, T. Wang, Z. Zhang, Powering future advancements and applications of battery energy storage systems across different scales, Energy Storage Appl. 2 (1) (Jan. 2025) 1, https://doi.org/10.3390/esa2010001.
[13] Marguerre, Ueber ein neues Verfahren zur Aufspeicherung elektrischer Energie, Mitt. Ver. Elektrizitätswerke 354 (55) (1924) 27–35.
[14] A. Benato, A. Stoppato, Pumped thermal electricity storage: a technology overview, Therm. Sci. Eng. Progress 6 (Jun. 2018) 301–315, https://doi.org/10.1016/j.tsep.2018.01.017.
[15] L.J.R. Nunes, Carnot batteries for grid-scale energy storage: technologies and the potential valorization of biomass ash as thermal storage media, Energies 18 (16) (Aug. 2025) 4235, https://doi.org/10.3390/en18164235.
[16] S.S.M. Shamsi, S. Barberis, S. Maccarini, A. Traverso, Large scale energy storage systems based on carbon dioxide thermal cycles: a critical review, Renew. Sust. Energy Rev. 192 (Mar. 2024) 114245, https://doi.org/10.1016/j.rser.2023.114245.
[17] Ding Wenjin, Bauer Thomas, "Next-Gen Molten Salt TES Technology for Advanced Carnot Batteries," presented at the 4th International Workshop on Carnot Batteries, Stuttgart, Germany, Sep. 2024. https://orcid.org/0000-0003-4080-7944.
[18] O. Dumont, G.F. Frate, A. Pillai, S. Lecompte, M. De Paepe, V. Lemort, Carnot battery technology: a state-of-the-art review, J. Energy Storage 32 (Dec. 2020) 101756, https://doi.org/10.1016/j.est.2020.101756.
[19] P. Wang, Q. Li, S. Wang, Study of two thermally integrated pumped thermal electricity storage systems using distinct working fluid groups: performance comparison, Case Stud. Therm. Eng. 61 (Sep. 2024) 105103, https://doi.org/10.1016/j.csite.2024.105103.
[20] S. Hu, Z. Yang, J. Li, Y. Duan, Thermo-economic analysis of the pumped thermal energy storage with thermal integration in different application scenarios, Energy Convers. Manag. 236 (May 2021) 114072, https://doi.org/10.1016/j.enconman.2021.114072.
[21] bccresearch, Carnot Battery: Transforming Energy Storage in the Future, Accessed: Feb. 24, 2026. [Online]. Available: https://www.bccresearch.com/industry-trends/carnot-battery-industry-trends-analysis, October 30, 2025.
[22] S. Zhang, Y. Sun, Innovative design and behavior investigation of the Carnot battery energy storage system: A pathway towards efficient utilization of renewable energy, Appl. Therm. Eng. 281 (Dec. 2025) 128581, https://doi.org/10.1016/j.applthermaleng.2025.128581.
[23] S. Zhang, Y. Lin, L. Zhou, H. Qian, J. Zhang, Y. Peng, Comparison of compressed air energy storage, compressed carbon dioxide energy storage, and Carnot battery: principles, thermal integration, and engineering demonstrations, Processes 13 (9) (Sep. 2025) 2882, https://doi.org/10.3390/pr13092882.
[24] X. Yan, C. Xu, M. Shao, Y. Yan, T. Dai, T. Xin, A comprehensive thermodynamic analysis of pumped thermal electricity storage systems: comparison between non-recuperated and recuperated configurations for various fluids, J. Energy Storage 127 (Aug. 2025) 117162, https://doi.org/10.1016/j.est.2025.117162.
[25] D. Qi, X. Feng, Y. Du, Y. Wu, B. Li, Thermodynamic analysis and optimization of pumped thermal electricity storage system of molten salt based on carbon dioxide Brayton cycle, Appl. Therm. Eng. 279 (Nov. 2025) 127773, https://doi.org/10.1016/j.applthermaleng.2025.127773.
[26] F. Wang, Q. He, Thermodynamic analysis of pump thermal energy storage system with different working fluid coupled biomass power plant, Energy 318 (Mar. 2025) 134758, https://doi.org/10.1016/j.energy.2025.134758.
[27] B. Eppinger, L. Zigan, J. Karl, S. Will, Pumped thermal energy storage with heat pump-ORC-systems: comparison of latent and sensible thermal storages for various fluids, Appl. Energy 280 (Dec. 2020) 115940, https://doi.org/10.1016/j.apenergy.2020.115940.
[28] Y.Q. Ge, Y. Zhao, C.Y. Zhao, Transient simulation and thermodynamic analysis of pumped thermal electricity storage based on packed-bed latent heat/cold stores, Renew. Energy 174 (Aug. 2021) 939–951, https://doi.org/10.1016/j.renene.2021.04.094.
[29] H. Yang, J. Wu, X. Du, Thermo-economic analysis and multi-objective optimization of solar aided pumped thermal electricity storage system, J. Energy Storage 70 (Oct. 2023) 107994, https://doi.org/10.1016/j.est.2023.107994.
[30] X. Shi, Q. He, C. Lu, T. Wang, S. Cui, D. Du, Variable load modes and operation characteristics of closed Brayton cycle pumped thermal electricity storage system with liquid-phase storage, Renew. Energy 203 (Feb. 2023) 715–730, https://doi.org/10.1016/j.renene.2022.12.116.
[31] A. Albay, Z. Zhu, M. Mercangöz, Optimization-based state-of-charge management strategies for supercritical CO2 Brayton cycle pumped thermal energy storage systems, J. Energy Storage 111 (Mar. 2025) 115387, https://doi.org/10.1016/j.est.2025.115387.
[32] H. Liu, Z. Wang, Z. Hou, M. Wang, Y. Ji, F. Han, Optimal design and performance analysis of a multi-temperature-zone cascaded cryogenic-synergized Carnot battery system, J. Energy Storage 133 (Oct. 2025) 117971, https://doi.org/10.1016/j.est.2025.117971.
[33] X.J. Xue, C.Y. Zhao, Transient behavior and thermodynamic analysis of Brayton-like pumped-thermal electricity storage based on packed-bed latent heat/cold stores, Appl. Energy 329 (Jan. 2023) 120274, https://doi.org/10.1016/j.apenergy.2022.120274.
[34] J. Jiang, B. Hu, R.Z. Wang, N. Deng, F. Cao, C.-C. Wang, A review and perspective on industry high-temperature heat pumps, Renew. Sust. Energy Rev. 161 (Jun. 2022) 112106, https://doi.org/10.1016/j.rser.2022.112106.

[35] K. Hamid, et al., Potential evaluation of integrated high temperature heat pumps: a review of recent advances, Appl. Therm. Eng. 230 (Jul. 2023) 120720, https://doi.org/10.1016/j.applthermaleng.2023.120720.
[36] M. Cascetta, F. Licheri, R.P. Merchán, M. Petrollese, Operating performance of a joule-Brayton pumped thermal energy storage system integrated with a concentrated solar power plant, J. Energy Storage 73 (Dec. 2023) 108865, https://doi.org/10.1016/j.est.2023.108865.
[37] M. Du, H. Yang, X. Du, H. Wu, Performance analysis of Carnot battery pumped thermal electricity storage aided with concentrated solar thermal input, Energy 319 (Mar. 2025) 135015, https://doi.org/10.1016/j.energy.2025.135015.
[38] S. Barberis, S.S.M. Shamsi, A. Traverso, Sco2-based thermally integrated-pumped thermal energy storage (Ti-Ptes) integrating freely available heat sources in both charging and discharging cycles, Energy 334 (Oct. 2025) 137608, https://doi.org/10.1016/j.energy.2025.137608.
[39] M. Petrollese, M. Cascetta, V. Tola, D. Cocco, G. Cau, Pumped thermal energy storage systems integrated with a concentrating solar power section: conceptual design and performance evaluation, Energy 247 (May 2022) 123516, https://doi.org/10.1016/j.energy.2022.123516.
[40] J. Yu, et al., Carnot battery with open-cycle ultra-high-temperature heat pump for large-scale hybrid PV and concentrating solar power plants, Energy 335 (Oct. 2025) 138385, https://doi.org/10.1016/j.energy.2025.138385.
[41] H. Zhang, L. Wang, X. Lin, H. Chen, Combined cooling, heating, and power generation performance of pumped thermal electricity storage system based on Brayton cycle, Appl. Energy 278 (Nov. 2020) 115607, https://doi.org/10.1016/j.apenergy.2020.115607.
[42] Y. Zhao, J. Huang, J. Song, Y. Ding, Thermodynamic investigation of a Carnot battery based multi-energy system with cascaded latent thermal (heat and cold) energy stores, Energy 296 (Jun. 2024) 131148, https://doi.org/10.1016/j.energy.2024.131148.
[43] A. Ghilardi, G.F. Frate, K. Kyprianidis, M. Tucci, L. Ferrari, Brayton pumped thermal energy storage: optimal dispatchment in multi-energy districts, Energy Convers. Manag. 314 (Aug. 2024) 118650, https://doi.org/10.1016/j.enconman.2024.118650.
[44] R. Sun, Y. Zhao, M. Liu, J. Yan, Thermodynamic design and optimization of pumped thermal electricity storage systems using supercritical carbon dioxide as the working fluid, Energy Convers. Manag. 271 (Nov. 2022) 116322, https://doi.org/10.1016/j.enconman.2022.116322.
[45] W.-D. Steinmann, D. Bauer, H. Jockenhöfer, M. Johnson, Pumped thermal energy storage (PTES) as smart sector-coupling technology for heat and electricity, Energy 183 (Sep. 2019) 185–190, https://doi.org/10.1016/j.energy.2019.06.058.
[46] H. Qiao, B. Yang, X. Yu, Development of an efficient cross-scale model for working fluid selection of Rankine-based Carnot battery based on group contribution method, Renew. Energy 238 (Jan. 2025) 121961, https://doi.org/10.1016/j.renene.2024.121961.
[47] G.F. Frate, L. Ferrari, U. Desideri, Multi-criteria investigation of a pumped thermal electricity storage (PTES) system with thermal integration and sensible heat storage, Energy Convers. Manag. 208 (Mar. 2020) 112530, https://doi.org/10.1016/j.enconman.2020.112530.
[48] J. Li, X. Chen, J. Shen, Y. Zhang, D. Liu, Optimal heat storage temperature and performance of ORC-based Carnot battery at various application scenarios, Energy Convers. Manag. 318 (Oct. 2024) 118906, https://doi.org/10.1016/j.enconman.2024.118906.
[49] S. Daniarta, P. Kolasiński, A.R. Imre, Performance map and theoretical analysis of Carnot battery technology via novel reversible Rankine-based cycle, Energy Rep. 11 (Jun. 2024) 4500–4514, https://doi.org/10.1016/j.egyr.2024.04.024.
[50] E. Bellos, C. Tzivanidis, Z. Said, Investigation and optimization of a solar-assisted pumped thermal energy storage system with flat plate collectors, Energy Convers. Manag. 237 (Jun. 2021) 114137, https://doi.org/10.1016/j.enconman.2021.114137.
[51] C. Zhu, et al., Discharging via the low-pressure section of the thermal power plant: a new integrated Carnot battery concept and the performance evaluation, Energy 331 (Sep. 2025) 137079, https://doi.org/10.1016/j.energy.2025.137079.
[52] X. Yang, F. Xu, E. Sun, Q. Chen, J. Xu, Enhanced coupling of low-grade heat sources with Carnot battery through optimal temperature matching, Energy Convers. Manag. 339 (Sep. 2025) 119953, https://doi.org/10.1016/j.enconman.2025.119953.
[53] R. Dai, R. Tian, S. Zheng, M. Wei, Finite-time thermodynamic and economic analysis of Rankine Carnot battery based on life-cycle method, Appl. Therm. Eng. 230 (Jul. 2023) 120813, https://doi.org/10.1016/j.applthermaleng.2023.120813.
[54] P. Wang, Q. Li, S. Wang, C. He, J. Tang, Thermo-economic analysis and comparative study of different thermally integrated pumped thermal electricity storage systems, Renew. Energy 217 (Nov. 2023) 119150, https://doi.org/10.1016/j.renene.2023.119150.
[55] H. Jockenhöfer, W.-D. Steinmann, D. Bauer, Detailed numerical investigation of a pumped thermal energy storage with low temperature heat integration, Energy 145 (Feb. 2018) 665–676, https://doi.org/10.1016/j.energy.2017.12.087.
[56] W. Tian, H. Xi, Comparative analysis and optimization of pumped thermal energy storage systems based on different power cycles, Energy Convers. Manag. 259 (May 2022) 115581, https://doi.org/10.1016/j.enconman.2022.115581.
[57] R. Fan, H. Xi, Exergoeconomic optimization and working fluid comparison of low-temperature Carnot battery systems for energy storage, J. Energy Storage 51 (Jul. 2022) 104453, https://doi.org/10.1016/j.est.2022.104453.
[58] P. Wang, Q. Li, S. Wang, T. Xiao, C. Wu, Thermo-economic and life cycle assessment of pumped thermal electricity storage systems with integrated solar energy contemplating distinct working fluids, Energy Convers. Manag. 318 (Oct. 2024) 118895, https://doi.org/10.1016/j.enconman.2024.118895.
[59] L.X. Chen, P. Hu, P.P. Zhao, M.N. Xie, F.X. Wang, Thermodynamic analysis of a high temperature pumped thermal electricity storage (HT-PTES) integrated with a parallel organic Rankine cycle (ORC), Energy Convers. Manag. 177 (Dec. 2018) 150–160, https://doi.org/10.1016/j.enconman.2018.09.049.
[60] L. Wang, X. Lin, H. Zhang, L. Peng, X. Zhang, H. Chen, Analytic optimization of Joule–Brayton cycle-based pumped thermal electricity storage system, J. Energy Storage 47 (Mar. 2022) 103663, https://doi.org/10.1016/j.est.2021.103663.
[61] A. White, G. Parks, C.N. Markides, Thermodynamic analysis of pumped thermal electricity storage, Appl. Therm. Eng. 53 (2) (May 2013) 291–298, https://doi.org/10.1016/j.applthermaleng.2012.03.030.
[62] J.D. McTigue, A.J. White, C.N. Markides, Parametric studies and optimisation of pumped thermal electricity storage, Appl. Energy 137 (Jan. 2015) 800–811, https://doi.org/10.1016/j.apenergy.2014.08.039.
[63] H. Qiao, X. Yu, W. Kong, E. Baniasadi, B. Yang, Multi-criteria optimization and thermo-economic analysis of a heat pump-organic Rankine cycle Carnot battery system, Green Energy Resour. 1 (4) (Dec. 2023) 100045, https://doi.org/10.1016/j.gerr.2023.100045.
[64] P. Wang, Q. Li, S. Wang, Comparative study of an innovative coldly integrated pumped thermal electricity storage system: Thermo-economic assessment and multi-objective optimization, Appl. Therm. Eng. 257 (Dec. 2024) 124295, https://doi.org/10.1016/j.applthermaleng.2024.124295.
[65] Q. Iqbal, et al., Techno-economic comparison of high-temperature and sub-ambient temperature pumped-thermal electricity storage systems integrated with external heat sources, J. Energy Storage 89 (Jun. 2024) 111630, https://doi.org/10.1016/j.est.2024.111630.
[66] M. Zhang, et al., Configuration mapping of thermally integrated pumped thermal energy storage system, Energy Convers. Manag. 294 (Oct. 2023) 117561, https://doi.org/10.1016/j.enconman.2023.117561.
[67] X. Xia, C. Yang, B. Peng, E. Liang, T. Jiang, Z. Wang, Thermal storage configuration mapping of the thermally integrated-pumped thermal energy storage system under different external conditions, J. Energy Storage 132 (Oct. 2025) 117660, https://doi.org/10.1016/j.est.2025.117660.
[68] X. Yu, H. Qiao, B. Yang, H. Zhang, Thermal-economic and sensitivity analysis of different Rankine-based Carnot battery configurations for energy storage, Energy Convers. Manag. 283 (May 2023) 116959, https://doi.org/10.1016/j.enconman.2023.116959.
[69] D. Steger, M. Feist, E. Schlücker, Using a screw-type machine as reversible compressor–expander in a Carnot battery: an analytical study towards efficiency, Appl. Energy 316 (Jun. 2022) 118950, https://doi.org/10.1016/j.apenergy.2022.118950.
[70] M. Weitzer, D. Müller, D. Steger, A. Charalampidis, S. Karellas, J. Karl, Organic flash cycles in Rankine-based Carnot batteries with large storage temperature spreads, Energy Convers. Manag. 255 (Mar. 2022) 115323, https://doi.org/10.1016/j.enconman.2022.115323.
[71] M. Weitzer, D. Müller, J. Karl, Two-phase expansion processes in heat pump – ORC systems (Carnot batteries) with volumetric machines for enhanced off-design efficiency, Renew. Energy 199 (Nov. 2022) 720–732, https://doi.org/10.1016/j.renene.2022.08.143.
[72] X. Zhang, M. He, Y. Zhang, A review of research on the Kalina cycle, Renew. Sust. Energy Rev. 16 (7) (Sep. 2012) 5309–5318, https://doi.org/10.1016/j.rser.2012.05.040.
[73] M. Soltani, M.H. Nabat, A.R. Razmi, M.B. Dusseault, J. Nathwani, A comparative study between ORC and Kalina based waste heat recovery cycles applied to a green compressed air energy storage (CAES) system, Energy Convers. Manag. 222 (Oct. 2020) 113203, https://doi.org/10.1016/j.enconman.2020.113203.
[74] A. Koen, P. Farres-Antunez, J. Macnaghten, A. White, A low-temperature glide cycle for pumped thermal energy storage, J. Energy Storage 42 (Oct. 2021) 103038, https://doi.org/10.1016/j.est.2021.103038.
[75] M.I. Aoki, K. Matsuda, M. Nakaiwa, C. Fushimi, Design and evaluation of a geothermal power plant integrated with $Mg(OH)_2/MgO$ thermochemical energy storage system: a dynamic simulation for assessing flexibility in power generation, energy, and economics, Chem. Eng. Sci. 299 (Nov. 2024) 120502, https://doi.org/10.1016/j.ces.2024.120502.
[76] X. Lu, A. Watson, J. Deans, Analysis of the thermodynamic performance of Kalina cycle system 11 (KCS11) for geothermal power plant: Comparison with Kawerau ORMAT binary plant, in: ASME 2009 3rd International Conference on Energy Sustainability Volume 1, ASMEDC, San Francisco, California, USA, Jan. 2009, pp. 357–358, https://doi.org/10.1115/ES2009-90165.
[77] T. Eller, F. Heberle, D. Brüggemann, Second law analysis of novel working fluid pairs for waste heat recovery by the Kalina cycle, Energy 119 (Jan. 2017) 188–198, https://doi.org/10.1016/j.energy.2016.12.081.
[78] P. Bombarda, C.M. Invernizzi, C. Pietra, Heat recovery from diesel engines: a thermodynamic comparison between Kalina and ORC cycles, Appl. Therm. Eng. 30 (2–3) (Feb. 2010) 212–219, https://doi.org/10.1016/j.applthermaleng.2009.08.006.
[79] Z. Guzović, D. Lončar, N. Ferdelji, Possibilities of electricity generation in the Republic of Croatia by means of geothermal energy, Energy 35 (8) (Aug. 2010) 3429–3440, https://doi.org/10.1016/j.energy.2010.04.036.
[80] A. Laterre, "Carnot Batteries for Heat and Power Coupling: Energy, Exergy, Economic and Environmental (4E) Analysis," Doctor, Universite de Liege, Belgium [Online]. Available: https://www.proquest.com/dissertations-theses/carnot-batteries-heat-power-coupling-energy/docview/3235011019/se-2, 2025.

[81] Q. Yong, K. Jin, X. Li, R. Yang, Thermo-economic analysis for a novel grid-scale pumped thermal electricity storage system coupled with a coal-fired power plant, Energy 280 (Oct. 2023) 128109, https://doi.org/10.1016/j.energy.2023.128109.
[82] M. Nilsson, Simplified pumped thermal energy storage using a two-way Stirling cycle, J. Energy Storage 73 (Dec. 2023) 108994, https://doi.org/10.1016/j.est.2023.108994.
[83] M. Nilsson, J. Jamot, T. Malm, "Operational data and thermodynamic modeling of a Stirling-dish demonstration installation in desert conditions," Presented at the SOLARPACES 2016: International Conference on Concentrating Solar Power and Chemical Energy Systems, Abu Dhabi, United Arab Emirates, 2017 050004, https://doi.org/10.1063/1.4984408.
[84] M. Nilsson, A. Abou-Taouk, H. Sandberg, J. Lindh, "A Stirling engine for thermal energy storage," Presented at the SOLARPACES 2018: International Conference on Concentrating Solar Power and Chemical Energy Systems, Casablanca, Morocco, 2019 140005, https://doi.org/10.1063/1.5117653.
[85] T. Lindquist, et al., "A novel modular and dispatchable CSP Stirling system: Design, validation, and demonstration plans," Presented at the SOLARPACES 2018: International Conference on Concentrating Solar Power and Chemical Energy Systems, Casablanca, Morocco, 2019 060005, https://doi.org/10.1063/1.5117591.
[86] J.E. Rea, et al., Prototype latent heat storage system with aluminum-silicon as a phase change material and a Stirling engine for electricity generation, Energy Convers. Manag. 199 (Nov. 2019) 111992, https://doi.org/10.1016/j.enconman.2019.111992.
[87] R. Morgan, S. Nelmes, E. Gibson, G. Brett, Liquid air energy storage – analysis and first results from a pilot scale demonstration plant, Appl. Energy 137 (Jan. 2015) 845–853, https://doi.org/10.1016/j.apenergy.2014.07.109.
[88] J. Park, S. Cho, M. Qi, W. Noh, I. Lee, I. Moon, Liquid air energy storage coupled with liquefied natural gas cold energy: focus on efficiency, energy capacity, and flexibility, Energy 216 (Feb. 2021) 119308, https://doi.org/10.1016/j.energy.2020.119308.
[89] Y. Ding, Y. Li, L. Tong, L. Wang, Liquid air energy storage, in: Storing Energy, Elsevier, 2022, pp. 191–205, https://doi.org/10.1016/B978-0-12-824510-1.00014-3.
[90] A.B. Gallo, J.R. Simões-Moreira, H.K.M. Costa, M.M. Santos, E. Moutinho Dos Santos, Energy storage in the energy transition context: a technology review, Renew. Sust. Energy Rev. 65 (Nov. 2016) 800–822, https://doi.org/10.1016/j.rser.2016.07.028.
[91] L. Wang, et al., Thermodynamic analysis and optimization of pumped thermal–liquid air energy storage (PTLAES), Appl. Energy 332 (Feb. 2023) 120499, https://doi.org/10.1016/j.apenergy.2022.120499.
[92] W. Ai, et al., Dynamic characteristics of pumped thermal-liquid air energy storage system: modeling, analysis, and optimization, Energy 313 (Dec. 2024) 133776, https://doi.org/10.1016/j.energy.2024.133776.
[93] W. Ai, L. Wang, X. Lin, H. Zhang, J. Huang, H. Chen, Multivariate multi-objective collaborative optimization of pumped thermal-liquid air energy storage, J. Energy Storage 81 (Mar. 2024) 110257, https://doi.org/10.1016/j.est.2023.110257.
[94] J.H. Park, J.Y. Heo, J.I. Lee, Techno-economic study of nuclear integrated liquid air energy storage system, Energy Convers. Manag. 251 (Jan. 2022) 114937, https://doi.org/10.1016/j.enconman.2021.114937.
[95] A. Vecchi, Y. Li, Y. Ding, P. Mancarella, A. Sciacovelli, Liquid air energy storage (LAES): a review on technology state-of-the-art, integration pathways and future perspectives, Adv. Appl. Energy 3 (Aug. 2021) 100047, https://doi.org/10.1016/j.adapen.2021.100047.
[96] M. Qi, J. Park, I. Lee, I. Moon, Liquid air as an emerging energy vector towards carbon neutrality: a multi-scale systems perspective, Renew. Sust. Energy Rev. 159 (May 2022) 112201, https://doi.org/10.1016/j.rser.2022.112201.
[97] X. She, et al., Liquid air energy storage – a critical review, Renew. Sust. Energy Rev. 208 (Feb. 2025) 114986, https://doi.org/10.1016/j.rser.2024.114986.
[98] N. Sun, J. Zhang, Y. Zhang, T. Hu, C. Wang, Z. Guo, A review of advancements in liquid air energy storage: system architecture, integration strategies, and thermodynamic analysis, Renew. Sust. Energy Rev. 226 (Jan. 2026) 116240, https://doi.org/10.1016/j.rser.2025.116240.
[99] A. Jahnke, L. Strenge, C. Fleßner, N. Wolf, T. Jungnickel, F. Ziegler, First cycle simulations of the Honigmann process with $LiBr/H_2O$ and $NaOH/H_2O$ as working fluid pairs as a thermochemical energy storage, Int. J. Low-Carbon Tech. 8 (Suppl. 1) (Jul. 2013) i55–i61, https://doi.org/10.1093/ijlct/ctt022.
[100] E. Thiele, A. Jahnke, F. Ziegler, Efficiency of the Lamm–Honigmann thermochemical energy storage, Therm. Sci. Eng. Prog. 19 (Oct. 2020) 100606, https://doi.org/10.1016/j.tsep.2020.100606.
[101] E. Thiele, F. Ziegler, Thermal operation maps for Lamm–Honigmann thermochemical energy storage—a quasi-stationary model for process analysis, Processes 10 (5) (May 2022) 977, https://doi.org/10.3390/pr10050977.
[102] Y. Zhao, M. Liu, J. Song, C. Wang, J. Yan, C.N. Markides, Advanced exergy analysis of a joule-Brayton pumped thermal electricity storage system with liquid-phase storage, Energy Convers. Manag. 231 (Mar. 2021) 113867, https://doi.org/10.1016/j.enconman.2021.113867.
[103] G.-B. Wang, X.-R. Zhang, Thermodynamic analysis of a novel pumped thermal energy storage system utilizing ambient thermal energy and LNG cold energy, Energy Convers. Manag. 148 (Sep. 2017) 1248–1264, https://doi.org/10.1016/j.enconman.2017.06.044.
[104] W. Song, S. Ma, B. Cao, C. Guo, X. Ma, J. Liu, Experimental study of pumped thermal electricity storage system based on Rankine cycle, Appl. Therm. Eng. 277 (Oct. 2025) 126977, https://doi.org/10.1016/j.applthermaleng.2025.126977.
[105] S. Quoilin, M.V.D. Broek, S. Declaye, P. Dewallef, V. Lemort, Techno-economic survey of organic Rankine cycle (ORC) systems, Renew. Sust. Energy Rev. 22 (Jun. 2013) 168–186, https://doi.org/10.1016/j.rser.2013.01.028.
[106] J. Bao, L. Zhao, A review of working fluid and expander selections for organic Rankine cycle, Renew. Sust. Energy Rev. 24 (Aug. 2013) 325–342, https://doi.org/10.1016/j.rser.2013.03.040.
[107] M. Weitzer, S. Reiß, D. Steger, S. Kolb, J. Karl, Experimental characterization of a reversible heat pump – organic Rankine cycle pilot plant as a thermally integrated Carnot battery, Appl. Therm. Eng. 260 (Feb. 2025) 124872, https://doi.org/10.1016/j.applthermaleng.2024.124872.
[108] Z. Wang, R. Xia, Y. Jiang, M. Cao, Y. Ji, F. Han, Evaluation and optimization of an engine waste heat assisted Carnot battery system for ocean-going vessels during harbor stays, J. Energy Storage 73 (Dec. 2023) 108866, https://doi.org/10.1016/j.est.2023.108866.
[109] D. Steger, C. Regensburger, J. Pham, E. Schlücker, Heat exchangers in Carnot batteries: condensation and evaporation in a reversible device, Energies 14 (18) (Sep. 2021) 5620, https://doi.org/10.3390/en14185620.
[110] Y. Li, P. Hu, H. Ni, Thermal-economic analysis and optimization of a novel segmented energy storage Carnot battery, Appl. Therm. Eng. 266 (May 2025) 125713, https://doi.org/10.1016/j.applthermaleng.2025.125713.
[111] H. Zhang, L. Wang, X. Lin, H. Chen, Parametric optimisation and thermo-economic analysis of Joule–Brayton cycle-based pumped thermal electricity storage system under various charging–discharging periods, Energy 263 (Jan. 2023) 125908, https://doi.org/10.1016/j.energy.2022.125908.
[112] T.R. Davenne, B.M. Peters, An analysis of pumped thermal energy storage with de-coupled thermal stores, Front. Energy Res. 8 (Aug. 2020) 160, https://doi.org/10.3389/fenrg.2020.00160.
[113] A. Hu, et al., Performance analysis of recuperated Brayton pumped thermal electricity storage with staged compressors, Energy 316 (Feb. 2025) 134539, https://doi.org/10.1016/j.energy.2025.134539.
[114] J. Wang, et al., Optimal scheduling of distributed energy system in the industrial park based on pumped thermal energy storage (Carnot battery), J. Energy Storage 110 (Feb. 2025) 115278, https://doi.org/10.1016/j.est.2024.115278.
[115] J.D. McTigue, P. Farres-Antunez, K.S. J, C.N. Markides, A.J. White, Techno-economic analysis of recuperated joule-Brayton pumped thermal energy storage, Energy Convers. Manag. 252 (Jan. 2022) 115016, https://doi.org/10.1016/j.enconman.2021.115016.
[116] X. Xia, H. Li, Z. Wang, C. Yang, Q. Zuo, F. Zhu, Thermo-economic evaluation of Carnot battery integrated with high-temperature waste heat, Energy 335 (Oct. 2025) 137980, https://doi.org/10.1016/j.energy.2025.137980.
[117] G.F. Frate, A. Baccioli, L. Bernardini, L. Ferrari, Assessment of the off-design performance of a solar thermally-integrated pumped-thermal energy storage, Renew. Energy 201 (Dec. 2022) 636–650, https://doi.org/10.1016/j.renene.2022.10.097.
[118] D. Canpolat Tosun, E. Açıkkalp, O. Altuntas, A. Hepbasli, A.I. Palmero-Marrero, D. Borge-Diez, Dynamic performance and sustainability assessment of a PV driven Carnot battery, Energy 278 (Sep. 2023) 127769, https://doi.org/10.1016/j.energy.2023.127769.
[119] H. Yang, X. Du, Thermo-economic analysis and multi-objective optimization of pumped thermal electricity storage system with S-CO2 recompression Brayton cycle, J. Energy Storage 124 (Jul. 2025) 116821, https://doi.org/10.1016/j.est.2025.116821.
[120] K. Nithyanandam, R. Pitchumani, Thermal energy storage with heat transfer augmentation using thermosyphons, Int. J. Heat Mass Transf. 67 (Dec. 2013) 281–294, https://doi.org/10.1016/j.ijheatmasstransfer.2013.08.007.
[121] R. Dai, M. Wei, R. Tian, S. Zheng, Enhancing performance of Rankine Carnot battery through cascaded latent heat storage with non-uniform volume allocation, Renew. Energy 242 (Apr. 2025) 122472, https://doi.org/10.1016/j.renene.2025.122472.
[122] B. Cao, et al., Performance analysis and optimization of finned tube latent thermal energy storage in pumped thermal electricity storage system based on Rankine cycle, Appl. Therm. Eng. 279 (Nov. 2025) 128110, https://doi.org/10.1016/j.applthermaleng.2025.128110.
[123] M. Albert, Z. Ma, H. Bao, A.P. Roskilly, Operation and performance of Brayton pumped thermal energy storage with additional latent storage, Appl. Energy 312 (Apr. 2022) 118700, https://doi.org/10.1016/j.apenergy.2022.118700.
[124] Y. Zhao, Y. Xie, J. Song, K. Wang, L. Cui, H. Zhang, Second-law thermodynamic assessment of cascaded latent-heat stores for pumped-thermal electricity storage, Appl. Therm. Eng. 262 (Mar. 2025) 125290, https://doi.org/10.1016/j.applthermaleng.2024.125290.
[125] Y. Zhao, J. Song, C. Zhao, Y. Zhao, C.N. Markides, Thermodynamic investigation of latent-heat stores for pumped-thermal energy storage, J. Energy Storage 55 (Nov. 2022) 105802, https://doi.org/10.1016/j.est.2022.105802.
[126] M. Zamengo, K. Yoshida, J. Morikawa, Numerical evaluation of a Carnot battery system comprising a chemical heat storage/pump and a Brayton cycle, J. Energy Storage 41 (Sep. 2021) 102955, https://doi.org/10.1016/j.est.2021.102955.
[127] J. Chen, Y. Zhou, J. Liu, Y. Zhao, S. Zhang, J. Yan, Thermodynamic performance of CaCl2 absorption heat pump thermal energy storage system with triple storage tanks, Appl. Therm. Eng. 237 (Jan. 2024) 121713, https://doi.org/10.1016/j.applthermaleng.2023.121713.
[128] M. Pecchini, S. Peccolo, A. Benato, F. De Vanna, A. Stoppato, Analysis of the discharge process of a TES-based electricity storage system, J. Energy Storage 100 (Oct. 2024) 113518, https://doi.org/10.1016/j.est.2024.113518.
[129] A. Benato, Performance and cost evaluation of an innovative pumped thermal electricity storage power system, Energy 138 (Nov. 2017) 419–436, https://doi.org/10.1016/j.energy.2017.07.066.

[130] Y. Zhao, J. Song, M. Liu, K. Zhang, C.N. Markides, J. Yan, Multi-objective thermo-economic optimisation of joule-Brayton pumped thermal electricity storage systems: role of working fluids and sensible heat storage materials, Appl. Therm. Eng. 223 (Mar. 2023) 119972, https://doi.org/10.1016/j.applthermaleng.2023.119972.
[131] J. McTigue, Z. Ma, Analysis of pumped thermal energy storage using particle media integrated with concentrating solar power, Sol. Energy 292 (May 2025) 113436, https://doi.org/10.1016/j.solener.2025.113436.
[132] W. Wang, S. Xu, W. Ju, L. Shi, X. Dai, Optimization of Carnot battery systems under different decision criteria: configuration, working fluid and parameter, J. Energy Storage 125 (Jul. 2025) 116906, https://doi.org/10.1016/j.est.2025.116906.
[133] D. Chen, Z. Han, X. Han, P. Li, Design, operation, and case analyses of a novel thermodynamic system combining coal-fired cogeneration and decoupled Carnot battery using CO2 as working fluid, Energy Convers. Manag. 296 (Nov. 2023) 117680, https://doi.org/10.1016/j.enconman.2023.117680.
[134] J. Gonzalez-Ayala, D. Salomone-González, A. Medina, J.M.M. Roco, P.L. Curto-Risso, A. Calvo Hernández, Multicriteria optimization of Brayton-like pumped thermal electricity storage with liquid media, J. Energy Storage 44 (Dec. 2021) 103242, https://doi.org/10.1016/j.est.2021.103242.
[135] S.M. Hosseinnia, H. Ermagan, A. Sasmito, S. Poncet, L. Amiri, Two-stage transcritical high temperature CO2 heat pump for dual heating-cooling coupled with thermal energy storages, Appl. Therm. Eng. 279 (Nov. 2025) 127802, https://doi.org/10.1016/j.applthermaleng.2025.127802.
[136] S. Zheng, S. Li, M. Li, R. Dai, M. Wei, R. Tian, Experimental and numerical investigation of a rectangular finned-tube latent heat storage unit for Carnot battery, J. Energy Storage 71 (Nov. 2023) 108092, https://doi.org/10.1016/j.est.2023.108092.
[137] M. Abarr, B. Geels, J. Hertzberg, L.D. Montoya, Pumped thermal energy storage and bottoming system part a: concept and model, Energy 120 (Feb. 2017) 320–331, https://doi.org/10.1016/j.energy.2016.11.089.
[138] Y. Hu, E. Yao, L. Zhong, S. Wu, H. Zou, G. Xi, Techno-economic analysis of thermochemical-integrated pumped thermal energy storage system, J. Energy Storage 104 (Dec. 2024) 114394, https://doi.org/10.1016/j.est.2024.114394.
[139] J. Chen, B. Zhao, M. He, Y. Long, Construction and thermodynamic optimization of a transcritical pumped thermal energy storage system using ice slurry for cold storage, Energy 319 (Mar. 2025) 134829, https://doi.org/10.1016/j.energy.2025.134829.
[140] M.A. Rosen, Appropriate thermodynamic performance measures for closed systems for thermal energy storage, J. Solar Energy Eng. 114 (2) (May 1992) 100–105, https://doi.org/10.1115/1.2929986.
[141] H.O. Njoku, O.V. Ekechukwu, S.O. Onyegegbu, Analysis of stratified thermal storage systems: an overview, Heat Mass Transf. 50 (7) (Jul. 2014) 1017–1030, https://doi.org/10.1007/s00231-014-1302-8.
[142] X.J. Xue, Y. Zhao, C.Y. Zhao, Multi-criteria thermodynamic analysis of pumped-thermal electricity storage with thermal integration and application in electric peak shaving of coal-fired power plant, Energy Convers. Manag. 258 (Apr. 2022) 115502, https://doi.org/10.1016/j.enconman.2022.115502.
[143] H. Zhang, L. Wang, X. Lin, H. Chen, Operating mode of Brayton-cycle-based pumped thermal electricity storage system: constant compression ratio or constant rotational speed? Appl. Energy 343 (Aug. 2023) 121107 https://doi.org/10.1016/j.apenergy.2023.121107.
[144] J. Guo, L. Cai, J. Chen, Y. Zhou, Performance optimization and comparison of pumped thermal and pumped cryogenic electricity storage systems, Energy 106 (Jul. 2016) 260–269, https://doi.org/10.1016/j.energy.2016.03.053.
[145] Y. Zhang, Z. Yang, Comparative study on optimized round-trip efficiency of pumped thermal and pumped cryogenic electricity storages, Energy Convers. Manag. 238 (Jun. 2021) 114182, https://doi.org/10.1016/j.enconman.2021.114182.
[146] G.F. Frate, M. Antonelli, U. Desideri, A novel pumped thermal electricity storage (PTES) system with thermal integration, Appl. Therm. Eng. 121 (Jul. 2017) 1051–1058, https://doi.org/10.1016/j.applthermaleng.2017.04.127.
[147] L. Wang, X. Lin, H. Zhang, L. Peng, H. Chen, Brayton-cycle-based pumped heat electricity storage with innovative operation mode of thermal energy storage array, Appl. Energy 291 (Jun. 2021) 116821, https://doi.org/10.1016/j.apenergy.2021.116821.
[148] J. Guo, L. Cai, J. Chen, Y. Zhou, Performance evaluation and parametric choice criteria of a Brayton pumped thermal electricity storage system, Energy 113 (Oct. 2016) 693–701, https://doi.org/10.1016/j.energy.2016.07.080.
[149] A.H. Hassan, L. O'Donoghue, V. Sánchez-Canales, J.M. Corberán, J. Payá, H. Jockenhöfer, Thermodynamic analysis of high-temperature pumped thermal energy storage systems: refrigerant selection, performance and limitations, Energy Rep. 6 (Dec. 2020) 147–159, https://doi.org/10.1016/j.egyr.2020.05.010.
[150] P. Wang, Q. Li, S. Wang, C. He, C. Wu, Off-design performance evaluation of thermally integrated pumped thermal electricity storage systems with solar energy, Energy Convers. Manag. 301 (Feb. 2024) 118001, https://doi.org/10.1016/j.enconman.2023.118001.
[151] L. Chen, et al., Thermo-economic analysis of a pumped thermal energy storage combining cooling, heating and power system coupled with photovoltaic thermal collector: exploration of low-grade thermal energy storage, J. Energy Storage 96 (Aug. 2024) 112718, https://doi.org/10.1016/j.est.2024.112718.
[152] P. Li, H. Yin, H. Li, Y. Yang, Z. Han, Thermo-economic performance assessment and multi-objective optimization of Carnot batteries with thermal integration, J. Energy Storage 125 (Jul. 2025) 117036, https://doi.org/10.1016/j.est.2025.117036.
[153] R. Smith, Chemical Process: Design and Integration, John Wiley & Sons, 2005.
[154] S. Hu, J. Li, F. Yang, Z. Yang, Y. Duan, How to design organic Rankine cycle system under fluctuating ambient temperature: a multi-objective approach, Energy Convers. Manag. 224 (Nov. 2020) 113331, https://doi.org/10.1016/j.enconman.2020.113331.
[155] W. Hill Balliet, P. Balducci, V. Durvasulu, T. Mosier, Determining the profitability of energy storage over its life cycle using levelized cost of storage, Energy Econ. 142 (Feb. 2025) 108174, https://doi.org/10.1016/j.eneco.2024.108174.
[156] C. Lu, et al., Dynamic modeling and numerical investigation of novel pumped thermal electricity storage system during startup process, J. Energy Storage 55 (Nov. 2022) 105409, https://doi.org/10.1016/j.est.2022.105409.
[157] J. McTigue, T. Neises, Off-design operation and performance of pumped thermal energy storage, J. Energy Storage 99 (Oct. 2024) 113355, https://doi.org/10.1016/j.est.2024.113355.
[158] K. Wang, X. Shi, Q. He, Thermodynamic analysis of novel carbon dioxide pumped-thermal energy storage system, Appl. Therm. Eng. 255 (Oct. 2024) 123969, https://doi.org/10.1016/j.applthermaleng.2024.123969.
[159] N. Wener, S. Martinez-Boggio, F. Favre, P. Curto-Risso, Zero-dimensional model of a pumped heat energy storage system with reciprocating machines, Appl. Energy 372 (Oct. 2024) 123764, https://doi.org/10.1016/j.apenergy.2024.123764.
[160] S. Rech, P. Danieli, G. Carraro, A. Lazzaretto, Multi-objective optimization of pumped thermal energy storage for large scale applications, Energy 334 (Oct. 2025) 137607, https://doi.org/10.1016/j.energy.2025.137607.
[161] A. Benato, A. Stoppato, Heat transfer fluid and material selection for an innovative pumped thermal electricity storage system, Energy 147 (Mar. 2018) 155–168, https://doi.org/10.1016/j.energy.2018.01.045.
[162] H. Wang, et al., Dynamic thermodynamic performance analysis of a novel pumped thermal electricity storage (N-PTES) system coupled with liquid piston, J. Energy Storage 84 (Apr. 2024) 110836, https://doi.org/10.1016/j.est.2024.110836.
[163] S. Parisi, R. Agromayor, A. La Seta, K.K. Nielsen, F. Haglind, Advancing non-dimensional models for radial turbomachinery applied to pumped thermal energy storage, Energy Convers. Manag. 342 (Oct. 2025) 120085, https://doi.org/10.1016/j.enconman.2025.120085.
[164] J. McTigue, J. Hirschey, Z. Ma, Advancing pumped thermal energy storage performance and cost using silica storage media, Appl. Energy 387 (Jun. 2025) 125567, https://doi.org/10.1016/j.apenergy.2025.125567.
[165] H. Zhang, L. Wang, X. Lin, H. Chen, Technical and economic analysis of Brayton-cycle-based pumped thermal electricity storage systems with direct and indirect thermal energy storage, Energy 239 (Jan. 2022) 121966, https://doi.org/10.1016/j.energy.2021.121966.
[166] J. Martinek, J. Jorgenson, J.D. McTigue, On the operational characteristics and economic value of pumped thermal energy storage, J. Energy Storage 52 (Aug. 2022) 105005, https://doi.org/10.1016/j.est.2022.105005.
[167] X.J. Xue, H.N. Wang, J.H. Wang, B. Yang, J. Yan, C.Y. Zhao, Experimental and numerical investigation on latent heat/cold stores for advanced pumped-thermal energy storage, Energy 300 (Aug. 2024) 131490, https://doi.org/10.1016/j.energy.2024.131490.
[168] Y. Zhao, et al., Thermo-economic assessments of pumped-thermal electricity storage systems employing sensible heat storage materials, Renew. Energy 186 (Mar. 2022) 431–456, https://doi.org/10.1016/j.renene.2022.01.017.
[169] S. Girelli, D. Alfani, E. Morosini, M. Astolfi, Optimal design of CO2 Carnot battery technology for long duration energy storage, Energy Convers. Manag. 344 (Nov. 2025) 120269, https://doi.org/10.1016/j.enconman.2025.120269.
[170] V.D. Stevanovic, L.O. Nord, M.A. Lazarevic, S. Milivojevic, M.M. Petrovic, N. Stevanovic, Carnot battery with steam accumulator and pebble bed thermal energy storage, Energy 329 (Aug. 2025) 136760, https://doi.org/10.1016/j.energy.2025.136760.
[171] Z. Liu, K. Zheng, C. Bai, X. Yan, Y. Zhang, Feasibility of transcritical pumped thermal energy storage system bottoming at ambient temperature, Appl. Therm. Eng. 268 (Jun. 2025) 126000, https://doi.org/10.1016/j.applthermaleng.2025.126000.
[172] Z. Liu, et al., Operation characteristics analysis of a trans-critical CO2 pumped thermal energy storage system, Appl. Therm. Eng. 279 (Nov. 2025) 127591, https://doi.org/10.1016/j.applthermaleng.2025.127591.
[173] Z. Liu, Y. Zhang, Y. Zhang, C. Su, Performance of a high-temperature transcritical pumped thermal energy storage system based on CO2 binary mixtures, Energy 305 (Oct. 2024) 132300, https://doi.org/10.1016/j.energy.2024.132300.
[174] K. Risthaus, R. Madlener, Economic analysis of electricity storage based on heat pumps and thermal storage units in large-scale thermal power plants, Energy Procedia 142 (Dec. 2017) 2816–2823, https://doi.org/10.1016/j.egypro.2017.12.427.
[175] Y. Jiang, W. Su, C. Wu, S. Wang, Enhanced thermally integrated Carnot battery using low-GWP working fluid pair: multi-aspect analysis and multi-scale optimization, Appl. Energy 376 (Dec. 2024) 124226, https://doi.org/10.1016/j.apenergy.2024.124226.
[176] B. Kurşun, K. Ökten, Improving the thermo-economic performance of a pumped thermal electricity storage (PTES) with a hybrid thermal integration scenario consisting of solar energy and waste heat, J. Energy Storage 103 (Dec. 2024) 114223, https://doi.org/10.1016/j.est.2024.114223.
[177] C. Yang, X. Xia, B. Peng, Z. Wang, H. Zhang, E. Liang, Multi-objective optimization and influence degree analysis of the thermally integrated HP-ORC Carnot battery based on the orthogonal design method and grey relational analysis, Energy 311 (Dec. 2024) 133360, https://doi.org/10.1016/j.energy.2024.133360.

[178] Z. Han, Y. Yang, P. Li, H. Yin, C. Zhou, Multi-objective optimization design of working fluids for Carnot battery system based on CAMD, J. Energy Storage 98 (Sep. 2024) 113108, https://doi.org/10.1016/j.est.2024.113108.
[179] Y. Li, P. Hu, H. Ni, K. Mu, Y. Ma, Performance analysis and optimisation of waste heat recovery system based on zeotropic working fluid, Appl. Therm. Eng. 253 (Sep. 2024) 123799, https://doi.org/10.1016/j.applthermaleng.2024.123799.
[180] B. Kurşun, K. Ökten, B. Özak, Reducing the cost of electricity storage with a novel solar thermal support scenario in pumped thermal energy storage (PTES), Appl. Therm. Eng. 241 (Mar. 2024) 122317, https://doi.org/10.1016/j.applthermaleng.2023.122317.
[181] Y. Zhang, J. Li, M. Yu, X. Chen, X. Chen, J. Shen, Dominant factor identification and fast optimization of Carnot battery by integrating SHAP and physics-guided neural network, Appl. Energy 401 (Dec. 2025) 126641, https://doi.org/10.1016/j.apenergy.2025.126641.
[182] C. Zhang, M. Li, C. Dang, X. Chen, X. Li, Z. Han, Enhanced Carnot battery for high-efficiency energy storage: feasibility analysis, Energy Convers. Manag. 332 (May 2025) 119754, https://doi.org/10.1016/j.enconman.2025.119754.
[183] J. Feng, Y. Yan, L. Zhao, H. Dong, Performance analysis and optimization of pumped thermal energy storage system coupled with low temperature waste heat recovery, J. Energy Storage 132 (Oct. 2025) 117968, https://doi.org/10.1016/j.est.2025.117968.
[184] X. Xia, et al., Sensitivity analysis of the system exergy performance of the thermally integrated-Carnot battery based on the orthogonal design method, Energy 335 (Oct. 2025) 137931, https://doi.org/10.1016/j.energy.2025.137931.
[185] O. Dumont, V. Lemort, Mapping of performance of pumped thermal energy storage (Carnot battery) using waste heat recovery, Energy 211 (Nov. 2020) 118963, https://doi.org/10.1016/j.energy.2020.118963.
[186] G.F. Frate, L. Ferrari, U. Desideri, Multi-criteria economic analysis of a pumped thermal electricity storage (PTES) with thermal integration, Front. Energy Res. 8 (Apr. 2020) 53, https://doi.org/10.3389/fenrg.2020.00053.
[187] P. Wang, et al., Comparative analysis of system performance of thermally integrated pumped thermal energy storage systems based on organic flash cycle and organic Rankine cycle, Energy Convers. Manag. 273 (Dec. 2022) 116416, https://doi.org/10.1016/j.enconman.2022.116416.
[188] B. Kurşun, K. Ökten, Comprehensive energy, exergy, and economic analysis of the scenario of supplementing pumped thermal energy storage (PTES) with a concentrated photovoltaic thermal system, Energy Convers. Manag. 260 (May 2022) 115592, https://doi.org/10.1016/j.enconman.2022.115592.
[189] H. Bahzad, P. Fennell, N. Shah, J. Hallett, N. Ali, Techno-economic assessment for a pumped thermal energy storage integrated with open cycle gas turbine and chemical looping technology, Energy Convers. Manag. 255 (Mar. 2022) 115332, https://doi.org/10.1016/j.enconman.2022.115332.
[190] K. Ökten, B. Kurşun, Thermo-economic assessment of a thermally integrated pumped thermal energy storage (TI-PTES) system combined with an absorption refrigeration cycle driven by low-grade heat source, J. Energy Storage 51 (Jul. 2022) 104486, https://doi.org/10.1016/j.est.2022.104486.
[191] L.M. Hadelu, A. Noorpoor, F.A. Boyaghchi, Assessment and multi-objective dragonfly optimization of utilizing flash tank vapor injection cycle in a new geothermal assisted-pumped thermal energy storage system based on transcritical CO2 cycle, J. Energy Storage 88 (May 2024) 111628, https://doi.org/10.1016/j.est.2024.111628.
[192] X. Sun, et al., Efficient and flexible thermal-integrated pumped thermal energy storage through composition adjustment, Carbon Neutrality 3 (1) (Dec. 2024) 11, https://doi.org/10.1007/s43979-024-00085-9.
[193] A. Ghilardi, A. Baccioli, G.F. Frate, M. Volpe, L. Ferrari, Integration of ocean thermal energy conversion and pumped thermal energy storage: system design, off-design and LCOS evaluation, Appl. Therm. Eng. 236 (Jan. 2024) 121551, https://doi.org/10.1016/j.applthermaleng.2023.121551.
[194] L. Migliari, M. Petrollese, G. Cau, D. Cocco, Techno-economic assessment and grid impact of thermally-integrated pumped thermal energy storage (TI-PTES) systems coupled with photovoltaic plants for small-scale applications, J. Energy Storage 77 (Jan. 2024) 109898, https://doi.org/10.1016/j.est.2023.109898.
[195] Y. Yan, et al., Thermodynamic evaluation of a novel Rankine-based pumped thermal energy storage concept targeting thermal coordination and large temperature span, Energy Convers. Manag. 309 (Jun. 2024) 118439, https://doi.org/10.1016/j.enconman.2024.118439.
[196] Y. Zhang, J. Liu, Z. Liu, Thermo-economic examination of ocean heat-assisted pumped thermal energy storage system using transcritical CO2 cycles, Appl. Therm. Eng. 255 (Oct. 2024) 123992, https://doi.org/10.1016/j.applthermaleng.2024.123992.
[197] M. Zhang, et al., Breaking the performance limitation of thermally integrated pumped thermal energy storage system: a three-way efficiency-boosting method, Energy Convers. Manag. 344 (Nov. 2025) 120276, https://doi.org/10.1016/j.enconman.2025.120276.
[198] S. Yin, C. Bai, K. Zheng, Y. Zhang, X. Yan, Z. Liu, Geothermal energy-assisted pumped thermal energy storage: configuration mapping, Energy Convers. Manag. 329 (Apr. 2025) 119660, https://doi.org/10.1016/j.enconman.2025.119660.
[199] C. Yang, X. Xia, C. Sun, B. Peng, J. Wu, Z. Wang, Single-objective and multi-objective optimization of the thermally integrated-pumped thermal energy storage system based on the novel optimization method coupling the orthogonal design and intelligent algorithm, Appl. Therm. Eng. 272 (Aug. 2025) 126404, https://doi.org/10.1016/j.applthermaleng.2025.126404.
[200] A.A. Alnaqi, J. Alsarraf, A.A.A.A. Al-Rashed, Thermodynamic and economic evaluation with multi-objective optimization of a novel thermally integrated pumped thermal energy storage system, Therm. Sci. Eng. Progress 58 (Feb. 2025) 103211, https://doi.org/10.1016/j.tsep.2025.103211.
[201] X.-Y. Tian, L.-K. Ba, X. Na, N. Chen, B.-W. Li, L. Chen, Thermo-economic assessment and optimization of thermally integrated pumped thermal energy storage with vapor-extraction regeneration, J. Energy Storage 113 (Mar. 2025) 115673, https://doi.org/10.1016/j.est.2025.115673.
[202] P. Lu, et al., Thermodynamic analysis and evaluation of a novel composition adjustable Carnot battery under variable operating scenarios, Energy Convers. Manag. 269 (Oct. 2022) 116117, https://doi.org/10.1016/j.enconman.2022.116117.
[203] H. Qiao, X. Yu, B. Yang, Working fluid design and performance optimization for the heat pump-organic Rankine cycle Carnot battery system based on the group contribution method, Energy Convers. Manag. 293 (Oct. 2023) 117459, https://doi.org/10.1016/j.enconman.2023.117459.
[204] T. Zhou, et al., Performance enhancement of thermal-integrated Carnot battery through zeotropic mixtures, Energy 311 (Dec. 2024) 133328, https://doi.org/10.1016/j.energy.2024.133328.
[205] D. Wu, et al., Working fluid pair selection of thermally integrated pumped thermal electricity storage system for waste heat recovery and energy storage, Appl. Energy 371 (Oct. 2024) 123693, https://doi.org/10.1016/j.apenergy.2024.123693.
[206] R. Dai, M. Wei, R. Tian, Thermodynamic and advanced exergy analysis of Rankine Carnot battery with cascaded latent heat storage, Appl. Therm. Eng. 258 (Jan. 2025) 124580, https://doi.org/10.1016/j.applthermaleng.2024.124580.
[207] M. Santos, J. André, R. Mendes, J.B. Ribeiro, Thermo-economic optimization of a Carnot battery under transient conditions, Appl. Therm. Eng. 269 (Jun. 2025) 126080, https://doi.org/10.1016/j.applthermaleng.2025.126080.
[208] Z. Liang, et al., Thermodynamic performance of organic rankine cycle based pumped thermal energy storage system with different working fluids, Heliyon 11 (1) (Jan. 2025) e41052, https://doi.org/10.1016/j.heliyon.2024.e41052.
[209] H. Mehmood, S. Teng, H. Xi, Thermo-economic parametric evaluation of different configurations of pumped thermal energy storage system using zeotropic fluids, J. Energy Storage 131 (Sep. 2025) 117517, https://doi.org/10.1016/j.est.2025.117517.
[210] M. Zhang, et al., Experimental investigation of thermally integrated Carnot battery system, J. Energy Storage 131 (Sep. 2025) 117618, https://doi.org/10.1016/j.est.2025.117618.
[211] P. Farres-Antunez, H. Xue, A.J. White, Thermodynamic analysis and optimisation of a combined liquid air and pumped thermal energy storage cycle, J. Energy Storage 18 (Aug. 2018) 90–102, https://doi.org/10.1016/j.est.2018.04.016.
[212] J. Du, et al., Efficiency enhancement of liquid air energy storage systems through ultra-high-temperature heat pump integration, Energy Convers. Manag. 332 (May 2025) 119714, https://doi.org/10.1016/j.enconman.2025.119714.
[213] J. Li, et al., Energy, exergy, and economic analyses of a novel liquid air and pumped thermal combined energy storage system, Energy Convers. Manag. 330 (Apr. 2025) 119675, https://doi.org/10.1016/j.enconman.2025.119675.
[214] S. Georgiou, N. Shah, C.N. Markides, A thermo-economic analysis and comparison of pumped-thermal and liquid-air electricity storage systems, Appl. Energy 226 (Sep. 2018) 1119–1133, https://doi.org/10.1016/j.apenergy.2018.04.128.
[215] S. Georgiou, M. Aunedi, G. Strbac, C.N. Markides, On the value of liquid-air and pumped-thermal electricity storage systems in low-carbon electricity systems, Energy 193 (Feb. 2020) 116680, https://doi.org/10.1016/j.energy.2019.116680.
[216] Q. Iqbal, et al., Thermo-economic assessment of sub-ambient temperature pumped-thermal electricity storage integrated with external heat sources, Energy Convers. Manag. 285 (Jun. 2023) 116987, https://doi.org/10.1016/j.enconman.2023.116987.
[217] W. Li, L. Zhang, Y. Deng, M. Zeng, Thermo-economic assessment of a salt hydrate thermochemical energy storage-based Rankine Carnot battery system, Energy Convers. Manag. 312 (Jul. 2024) 118564, https://doi.org/10.1016/j.enconman.2024.118564.
[218] J. Niu, J. Wang, X. Liu, L. Dong, Optimal integration of solar collectors to Carnot battery system with regenerators, Energy Convers. Manag. 277 (Feb. 2023) 116625, https://doi.org/10.1016/j.enconman.2022.116625.
[219] S. Liu, H. Bai, P. Jiang, Q. Xu, M. Taghavi, Economic, energy and exergy assessments of a Carnot battery storage system: comparison between with and without the use of the regenerators, J. Energy Storage 50 (Jun. 2022) 104577, https://doi.org/10.1016/j.est.2022.104577.
[220] Z. Liu, et al., Thermal economy analysis and multi-objective optimization of a small CO2 transcritical pumped thermal electricity storage system, Energy Convers. Manag. 293 (Oct. 2023) 117451, https://doi.org/10.1016/j.enconman.2023.117451.
[221] Y. Zhang, S. Yin, X. Yan, Z. Liu, Performance of a CO2-based mixture cycled transcritical pumped thermal energy storage system, Renew. Energy 238 (Jan. 2025) 121893, https://doi.org/10.1016/j.renene.2024.121893.
[222] B. Kurşun, Comparison with Carnot battery of an alternate thermal electricity storage charged by concentrated photovoltaic thermal system and resistance heater, Appl. Therm. Eng. 258 (Jan. 2025) 124587, https://doi.org/10.1016/j.applthermaleng.2024.124587.
[223] ENERGYDOME, CO2 battery, Accessed: Feb. 24, 2026. [Online]. Available: https://energydome.com/co2-battery/, 2021.
[224] EPRI, Program on Technology Innovation: EPRI Insights: Long-Duration Storage–Emerging Pilot Project Summaries, EPRI, Palo Alto, CA, 2024 [Online]. Available, extension://ngbkcglbmlglgldjfcnhaijeecaccgfi/https://restservice.epri.com/publicdownload/000000003002029144/0/Product 3002028130.
[225] Everllence, Energy storage, Accessed: Feb. 24, 2026. [Online]. Available: https://www.everllence.com/energy/solutions/energy-storage/liquid-air-energy, 2026.
[226] 1414°, 1414° thermal energy storage system, Accessed: Feb. 24, 2026. [Online]. Available: https://1414degrees.com.au/sibox/, 2026.

[227] siemensgamesa, World first: Siemens Gamesa begins operation of its innovative electrothermal energy storage system, Accessed: Feb. 24, 2026. [Online]. Available: https://www.siemensgamesa.com/global/en/home/press-releases/190612-siemens-gamesa-inauguration-energy-system-thermal.html, June 12, 2019.
[228] V. Novotny, V. Basta, P. Smola, J. Spale, Review of Carnot battery technology commercial development, Energies 15 (2) (Jan. 2022) 647, https://doi.org/10.3390/en15020647.
[229] Stiesdal, "The GridScale storage system," The GridScale technology explained, Accessed: Feb. 24, 2026. [Online]. Available: https://www.stiesdal.com/storage/the-gridscale-technology-explained/, 2020.
[230] State Key Laboratory of Industrial Control Technology, "The ultra-high-temperature PTHS", Accessed: Feb. 24, 2026. [Online]. Available: https://sklict.zju.edu.cn/2025/0320/c85586a3029258/page.htm, March 20, 2025.
[231] China Energy Storage Network News Center, Green Storage Technology Supports Successful First Trial Run of 8MW/400°C Axial-Flow Ultra-High Temperature Heat Pump Thermal Energy Storage Demonstration Project in Xisai Science Valley to Commence Operation, Accessed: Feb. 24, 2026. [Online]. Available: https://www.escn.com.cn/news/show-2156056.html, December 28, 2025.
[232] Vincent Shaw, World-first 560°C Carnot battery unveiled as SPIC launches ultra-high-temperature heat storage, Accessed: Jun. 06, 2026. [Online]. Available: https://www.ess-news.com/2026/01/12/world-first-560c-carnot-battery-unveiled-as-spic-launches-ultra-high-temperature-heat-storage/#comments, Jan 12, 2026.
[233] Highview, Carrington, Manchester - GEN01X, Accessed: Feb. 24, 2026. [Online]. Available: https://highviewpower.com/projects/, 2025.
[234] E2S-power, "Thermal energy storage-TWEST," Our Product, Accessed: Feb. 24, 2026. [Online]. Available: https://e2s-power.com/our-product/, 2020.
[235] E2S-power, Thermal energy storage, production of CO2 free electricity in thermal power plants, Accessed: Feb. 24, 2026. [Online]. Available: https://e2s-power.com/thermal-energy-storage-production-of-co2-free-electricity-in-thermal-power-plants/, 2020.
[236] echogen, Grid-scale storage that doesn't wear out, Accessed: Feb. 24, 2026. [Online]. Available: https://www.echogen.com/technology/energy-storage, 2025.
[237] TEXEL, TEXEL Energy Storage, Accessed: Feb. 24, 2026. [Online]. Available: https://www.texelholding.com/texel-energy-storage-2/, 2026.
[238] windTP, windTP system, Accessed: Feb. 24, 2026. [Online]. Available: https://windtp.com/, 2026.
[239] Loz Blain, 'World's first working thermal battery' promises cheap, eco-friendly, grid-scalable energy storage, Accessed: Feb. 24, 2026. [Online]. Available: https://newatlas.com/cct-silicon-energy-battery-thermal-energy-storage/59098/, April 01, 2019.
[240] pintailpower, Liquid salt combined cycle, Accessed: Feb. 24, 2026. [Online]. Available: https://www.pintailpower.com/technology/liquid-salt-combined-cycle/, 2019.
[241] pintailpower, Liquid air combined cycle [Online]. Available: https://www.pintailpower.com/technology/liquid-air-combined-cycle/, Accessed: Feb. 24, 2026.
[242] Huan Zhu, Hu Li, Guojing Liu, Yi Ge, Jing Shi, Hai Li, Energy storage in high renewable penetration power systems: technologies, applications, supporting policies and suggestions, CSEE J. Power Energy Syst. (Jun. 2020), https://doi.org/10.17775/CSEEJPES.2020.00090.
[243] DFG, SPP 2403: Carnot-Batterien: Inverser Entwurf vom Markt bis zum Molekül, Accessed: Feb. 24, 2026. [Online]. Available: https://gepris.dfg.de/gepris/projekt/500600620?context=projekt&task=showDetail&id=500600620&, 2023.
[244] R. Tassenoy, A. Laterre, V. Lemort, F. Contino, M. De Paepe, S. Lecompte, Assessing the influence of compressor inertia on the dynamic performance of large-scale vapor compression heat pumps for Carnot batteries, J. Energy Storage 101 (Nov. 2024) 113948, https://doi.org/10.1016/j.est.2024.113948.
[245] I. Beyers, A. Bensmann, R. Hanke-Rauschenbach, A. Sciacovelli, Off-design operation of grid-scale pumped thermal energy storage: a comparative analysis of control strategies, J. Energy Storage 153 (Apr. 2026) 120626, https://doi.org/10.1016/j.est.2026.120626.
[246] T. Liang, et al., Key components for Carnot battery: technology review, technical barriers and selection criteria, Renew. Sust. Energy Rev. 163 (Jul. 2022) 112478, https://doi.org/10.1016/j.rser.2022.112478.
[247] G.F. Frate, M. Pettinari, E. Di Pino Incognito, R. Costanzi, L. Ferrari, Dynamic modelling of a Brayton PTES system, in: Volume 4: Cycle Innovations; Cycle Innovations: Energy Storage, American Society of Mechanical Engineers, Rotterdam, Netherlands, Jun. 2022 V004T07A013, https://doi.org/10.1115/GT2022-83445.
[248] Matteo Pecchini, Simone Peccolo, Anna Stoppato, Alberto Benato, "An ad hoc control system for managing the dynamic behaviour of a Brayton-based Carnot battery," presented at the 38th International Conference on Efficiency, Cost, Optimization, Simulation and Environmental Impact of Energy Systems, ECOS 2025, Mines Paris PSL University, Paris, 2025. Accessed: Jun. 06, 2026. [Online]. Available: https://www.scopus.com/pages/publications/105037438880.
[249] J. Huang, et al., Dynamic performance and control of Carnot battery-based combined cooling, heating and power systems with cascaded latent thermal energy stores, Appl. Energy 406 (Mar. 2026) 127286, https://doi.org/10.1016/j.apenergy.2025.127286.
[250] Y. Feng, et al., Dynamic behavior and control efficacy in Carnot battery systems: a comparative study of feedforward, PID, and combined control methods, Energy 337 (Nov. 2025) 138653, https://doi.org/10.1016/j.energy.2025.138653.
[251] B. Zhou, J. Yuan, J. Lu, F. Hong, Investigation on transient behavior of residual heat removal pumps in 1000 MW nuclear power plant using a 1D-3D coupling methodology during start-up period, Ann. Nucl. Energy 110 (Dec. 2017) 560–569, https://doi.org/10.1016/j.anucene.2017.07.013.
[252] G. Hu, L. Zou, D.J. O'Grady, R. Hu, An integrated coupling model for solving multiscale fluid-fluid coupling problems in SAM code, Nucl. Eng. Des. 404 (Apr. 2023) 112186, https://doi.org/10.1016/j.nucengdes.2023.112186.
[253] J. Li, Z. Jiang, Y. Zhao, X. Feng, M. Zheng, An optimal load distribution and real-time control strategy for integrated energy system based on nonlinear model predictive control, Energy 308 (Nov. 2024) 132878, https://doi.org/10.1016/j.energy.2024.132878.
[254] S. Naik, L. Ghilardi, R. Parker, L.T. Biegler, Multistage economic MPC for systems with a cyclic steady state: a gas network case study, Chem. Eng. Sci. 319 (Jan. 2026) 122276, https://doi.org/10.1016/j.ces.2025.122276.